TM-71-2034-1

TECHNICAL MEMORANDUM

A PHASE-LOCKED LOOP DEMODULATOR FOR TELEVISION TYPE PM SIGNALS

Bellcomm

BELLCOMM, INC.
955 L'ENFANT PLAZA NORTH, S.W., WASHINGTON, D.C. 20024

COVER SHEET FOR TECHNICAL MEMORANDUM

TITLE- A Phase-Locked Loop Demodulator for Television Type PM Signals

TM- 71-2034-1

DATE- May 5, 1971

FILING CASE NO(S)- 320

AUTHOR(S)- W. D. Wynn

FILING SUBJECT(S) (ASSIGNED BY AUTHOR(S))- Phase-Locked Loop
Phase Demodulation

ABSTRACT

This paper presents the development of a tractable suboptimum demodulator in a phase-locked loop configuration for demodulating a model of a television signal received as phase modulation on a sinusoidal carrier. One possible application of this development is in the Apollo Unified S-Band communication system where television is one of the subcarrier signals for some transmission modes employed. The available waveform at the demodulator input is assumed to be the sum of the phase modulated carrier and a stationary Gaussian noise. The suboptimum demodulator is suggested by using the Wiener spectrum factorization technique to find the transmission poles and zeros of the optimum linear loop filter. A simple linear filter is then shown to approximate the infinite number of optimum loop poles and zeros that arise due to the complicated signal model used. The demodulator developed is suboptimum in that its mean square error in forming a phase estimate is greater than that which is theoretically possible using realizable loop filters. Although the optimum demodulator is not derived, its mean square estimation error is computed and is compared to the estimation error for the suboptimum demodulator. This comparison is in terms of output signal-to-noise power ratios for the two demodulators as the input signal power-to-noise spectral density is varied. An important question about system stability is answered for the linear equivalent suboptimum demodulator obtained when the phase-locked loop is in lock.

SEE REVERSE SIDE FOR DISTRIBUTION LIST

DISTRIBUTION

COMPLETE MEMORANDUM TO

CORRESPONDENCE FILES:

OFFICIAL FILE COPY
plus one white copy for each additional case referenced

TECHNICAL LIBRARY (4)

NASA Headquarters
W. B. Evans/MLO
J. K. Holcomb/MAO
A. S. Lyman/MR
J. T. McClanahan/MAO
L. M. Robinson/TS
W. E. Stoney/MA

MSC
G. D. Arndt/EB2
E. L. Chicoine/EE3
H. C. Kyle/EB
C. K. Land/EB2
R. W. Moorehead/EB2
L. Packham/EE
R. S. Sawyer/EE
W. E. Zrubek/EE6

MSFC
T. A. Barr/PD-SS-M
J. B. Cox/S&E-ASTR-SC
H. R. Lowery/S&E-ASTR-SCD
L. B. Malone/S&E-ASTR-IR

GSFC
O. M. Covington/800
A. F. Grandinetti/834
T. Roberts/810
J. P. Shaughnessy/834
W. P. Varson/830

BTL
T. V. Crater/HO
C. C. Cutler/HO
C. G. Davis/HO
R. Lowell/HO
C. F. Simone/HO

Bellcomm, Inc.
G. M. Anderson
W. J. Benden
A. P. Boysen. Jr.
K. R. Carpenter
R. K. Chen
J. P. Downs*
L. A. Ferrara
D. R. Hagner
H. A. Helm
J. J. Hibbert
J. E. Johnson
H. Kraus
S. Y. Lee
D. P. Ling
J. P. Maloy
J. Z. Menard
L. D. Nelson
J. T. Raleigh
I. I. Rosenblum
N. W. Schroeder
R. V. Sperry
J. L. Strand
J. W. Timko
R. L. Wagner
A. G. Weygand
M. P. Wilson
Department 1024 File

*Abstract Only

BA-146 (8-64)

BELLCOMM, INC.
955 L'ENFANT PLAZA NORTH, S.W. WASHINGTON, D. C. 20024

SUBJECT: A Phase-Locked Loop Demodulator for Television Type PM Signals Case 320

DATE: May 5, 1971

FROM: W. D. Wynn

TM-71-2034-1

TECHNICAL MEMORANDUM

(1.0) INTRODUCTION

In the following memorandum we will derive a phase demodulator of the phase locked loop (PLL) form that recovers a television type (TV) signal. This signal is received as phase modulation on a sinusoidal carrier in the presence of additive noise.

Starting with a mathematical model of the signal average power spectrum, we derive the PLL demodulator that yields the minimum mean square (mms) error estimate of the signal. We assume the additive noise received with the carrier has a uniform average power spectral density over the frequency band of the received PM waveform.

Due to the complex form of the signal power spectrum, the loop filter in the PLL that produces the mms error estimate of the signal is difficult to realize. We show that, for our assumed signal spectrum model, a simple transversal filter in the loop gives an estimate close to the theoretical mms error estimate.

The phase locked loop that gives the mms error estimate is a Wiener filter and it is obtained by the Wiener spectrum factorization technique. We find that the internal filter in the optimum PLL has countably infinite isolated poles and zeros in the left half of the s-plane. We derive a simple transversal filter with countably infinite isolated poles that can be adjusted so that the optimum PLL is closely approximated.

Our justification for selecting as a transmission mode the direct phase modulation of the signal onto the carrier is the following. For many kinds of signal spectra, PM is close to the optimum form of angle modulation when we are operating under a channel mean-square bandwidth constraint or a demodulator threshold constraint, and the criterion of performance used is mms error between the modulating signal and its estimate (Ref. 1).

The only criterion of performance we consider in this memorandum is mms error between the signal and the signal estimate. When the modulating signals spectrum is assumed to be that of a TV picture, the performance of the demodulator must be evaluated subjectively by the viewer, since the viewer is the sink for the TV information (Ref. 2). Based on subjective evaluation by the viewer, it is known that the optimum PM demodulator for a TV signal need not be the PM demodulator that produces a mms error estimate of the TV signal. The criterion of mms error can be misleading when applied to anything as subjective as TV picture quality (Ref. 3). If subjective effects in TV can be described in the frequency domain by weighting the power spectrum of the TV signal before transmission, the mms error optimization described in this memorandum can be adapted to give an accurate optimum demodulator for phase modulated TV.

(2.0) DISCUSSION

The essential components of the PM system we will consider are shown in Figure 1. The demodulator in this system is a phase locked loop with a post loop filter. The internal loop filter and the post loop filter are both assumed to be linear and time invariant (LTI). The Laplace domain transfer functions for these two filters are $F(s)$ and $F_o(s)$ as noted in Figure 1. In all cases the filters are assumed to be physically realizable.

We assume the channel interference to be additive stationary Gaussian noise with zero mean value. We also assume that the receiver IF filter is LTI and is sufficiently wideband compared to the significant spectrum of $s(t)$ that $n(t)$ is approximately white compared with $s(t)$. That is, the correlation interval of $n(t)$ is much shorter than the correlation interval of $s(t)$. Then $n(t)$ can be approximated by a white Gaussian noise with a two-sided power spectral density $N_o/2$.

(2.1) Baseband Model of PLL Demodulator

For proper demodulation of $\theta(t) = K_t\, m(t)$, the PLL reference $r(t)$ must "lock on" the incoming waveform $s(t)$ such that $\sin [\theta(t) - \hat{\theta}(t)] \simeq \theta(t) - \hat{\theta}(t)$ most of the time. Then the demodulator in Figure 1 is equivalent to the linear lowpass system in Figure 2. This is the above threshold model for the demodulator that is obtained if the ratio of signal power-to-noise spectral density, $2A^2/N_o$, is above a threshold value; and

the LPF F(s) is properly designed for $\theta(t)$ (Ref. 4, Sec. 5.5). In Figure 2 we have a new noise function $n'(t)/A$ related to the $n(t)$ in Figure 1. For a white noise $n(t)$ with two-sided density $N_o/2$, the function $n'(t)$ is also white with the same two-sided density $N_o/2$. Then $n'(t)/A$ is white with two-sided density $N_o/2A^2$. In Figure 2, H(s) is the closed loop transfer function between points (1) and (2), while T(s) is the overall transfer function between (1) and (4).

The criterion of performance we use is the mms error between the desired signal $\theta(t)$ and its estimate that is generated by our demodulator. The system in Figure 2 is linear. The transfer function H(s) that makes $\hat{\theta}(t)$ a mms error estimate of $\theta(t)$ is a realizable Wiener filter. The filter H(s) must operate on the input $\theta(\tau) + n'(\tau)/A$ for all $\tau \leq t$ to produce the estimate $\theta(t)$. If the transfer function H(s) was permitted to be unrealizable, we know that the mms error estimate of $\theta(t)$ is obtained when H(s) processes $\theta(\tau) + n'(\tau)/A$ for $-\infty < \tau < +\infty$ to form the estimate $\hat{\theta}(t)$. But if we attempt a realizable approximation to the unrealizable optimum filter by using time delay δ, we cannot maintain $\sin [\theta(t) - \hat{\theta}(t+\delta)] \simeq \theta(t) - \hat{\theta}(t+\delta)$; and hence our PLL will not stay locked onto the signal $\theta(t)$. Then H(s) must be a realizable Wiener filter with no time delay in forming the estimate $\hat{\theta}(t)$ (Ref. 4, Page 139).

Since the filter $F_o(s)$ is not part of the feedback loop in Figure 2, we can introduce time delay in this post loop filter and improve our estimate of $\theta(t)$. For a sufficiently long time delay in $F_o(s)$ we would process $\theta(\tau) + n'(\tau)/A$ for effectively the entire interval $-\infty < \tau < +\infty$ to produce the irreducible mms error estimate $\hat{\theta}_\infty(t)$ (Ref. 5, Sec. 6.2.3). The derivation of the optimum realizable $F_o(s)$ with delay is outlined in Appendix I.

Because of the complex nature of the TV type signal $\theta(t)$ to be considered here, it does not seem practical to construct an optimum realizable $F_o(s)$ with delay. However, we will find a fairly simple circuit for the optimum H(s).

(2.2) The Optimum Loop Filter

The realizable mms error filter that estimates $\theta(t)$ given $\theta(\tau) + n'(\tau)/A$, $\tau \leq t$, will be denoted by $H_o(s)$. For a white noise $n'(t)$ the expression for $H_o(s)$ has a simple form. If we let $N'' = N_o/2A^2$ be the two-sided power spectral density of $n'(t)/A$, we have

$$H_o(j\omega) = 1 - 1/\Psi(\omega) \tag{1}$$

where $$|\Psi(\omega)|^2 = \Psi(\omega)\ \Psi^*(\omega) = 1 + S_\theta(\omega)/N'' \tag{2}$$

and $\Psi(\omega)$ consists of all the poles and zeros of $|\Psi(\omega)|^2$ in the upper-half ω-plane (Ref. 4, Equation 5.110). The complex conjugate of $\Psi(\omega)$ is $\Psi^*(\omega)$.

The loop filter $F(s)$ that corresponds to $H_o(j\omega)$ follows directly from Figure 2. We denote this optimum loop filter by $F_{\ell op}(j\omega)$. Then

$$F_{\ell op}(j\omega) = \frac{1}{AK_r}\,[\Psi(\omega) - 1]. \tag{3}$$

To specify the optimum PLL demodulator for the mms error estimate of $\theta(t)$, all that is needed is the function $\Psi(\omega)$. However, for the signal $\theta(t)$ we want to consider, it is not easy to find $\Psi(\omega)$.

(2.3) Minimum Mean Square Error

With the realizable closed loop transfer function $H_o(j\omega)$, we get the mms error in estimating $\theta(t)$ with zero time delay. This error is (Ref. 5, Sec. 6.2.4)

$$\sigma_o^2 = \frac{N''}{2\pi} \int_{-\infty}^{+\infty} \ell n\ [1 + S_\theta(\omega)/N'']\ d\omega \tag{4}$$

When no time delay is permitted in estimating $\theta(t)$, the post loop filter $F_o(j\omega) = K_r$, a constant. If sufficient time delay is possible and the appropriate realizable filter $F_o(j\omega)$ is used, the estimate approaches $\hat{\theta}_\infty(t)$ and the estimation error approaches the irreducible mms error (Ref. 5, Sec. 6.2.3)

$$\sigma_\infty^2 = \frac{N''}{2\pi} \int_{-\infty}^{+\infty} \frac{S_\theta(\omega)}{S_\theta(\omega)+N''} \, d\omega. \tag{5}$$

(2.4) The Signal Spectrum Model

The signal $\theta(t)$ we consider in this memorandum is derived from the TV signal model due to L. E. Franks (Ref. 3, Sec. 5). The average signal power spectrum from Frank's model is given by

$$S(f) = (1-\alpha)\, G_h(f)\, G_v(f)\, G_t(f) + \bar{d}^2\, \delta(f)$$

$$+ \sum_{\ell=-\infty}^{+\infty} |W_\ell|^2\, \delta(f-\ell/NT) \tag{6}$$

Here $\delta(f-x)$ is the unit frequency domain impulse at $f = x$, $\bar{d}$ is the mean value of the picture luminance, W_ℓ is the $\ell^{\underline{th}}$ Fourier coefficient of the periodic (non-random) part of the signal, α is the fraction of the total signal time taken by the synchronizing and blanking signals; and NT is the time from the start of one frame to the start of the following frame.

The average signal power spectrum part due to random variations in the signal is modeled by the three factors $G_h(f)$, $G_v(f)$ and $G_t(f)$. These are defined by

$$G_h(f) = \left(\overline{d^2} - \bar{d}^2\right) \frac{2\,\lambda_h}{\omega^2 + \lambda_h^2}, \tag{7}$$

$$G_v(f) = \frac{\sinh\ (T_e\ \lambda_v)}{\cosh\ (T_e\ \lambda_v) - \cos\ \omega T}, \tag{8}$$

and

$$G_t(f) = \frac{\sinh\ (NT\ \lambda_t)}{\cosh\ (NT\ \lambda_t) - \cos\ (NT\omega)}, \tag{9}$$

where $\omega = 2\pi f$. The function $G_h(f)$ represents horizontal picture correlation element-to-element, the function $G_v(f)$ represents vertical picture correlation line-to-line; and the function $G_t(f)$ represents frame-to-frame correlation. The parameters in (7), (8), and (9) are defined in Appendix II.

A typical graph of $G_h\ G_v\ G_t$ is shown as the shaded part of Figure 3. The factor $G_h\ G_v$ acts as an envelope for the more rapidly oscillating G_t function. From (7) we see that the peaks of the envelope $G_h\ G_v$ decay with frequency as ω^{-2} for large ω.

Any filter optimization based on the signal model in (6) is complicated by the fine comb structure that G_t introduces. We can set $G_t = 1$ if there is no frame-to-frame correlation in the picture. In this case the envelope $G_h\ G_v$ becomes the spectrum of the random part of the signal model.

In this memorandum the signal $\theta(t)$ to be considered is derived from Franks' model by omitting frame-to-frame correlation and the non-random components from the model. The signal $\theta(t)$ then has the spectrum

$$S_\theta(\omega) = G_h\ G_v \tag{10}$$

where G_h and G_v are given in (7) and (8). The energy in $S_\theta(\omega)$ is concentrated at integer multiples of 1/T where T is the line scan interval in seconds (Appendix II).

(2.5) The Optimum Loop Filter for the Limiting Case $G_h = 1$.

From (3) the optimum loop filter $F_{\ell op}(j\omega)$ in Figure 2 is determined once we find $\Psi(\omega)$. As a preliminary step in finding $\Psi(\omega)$ for $S_\theta(\omega)$ in (10) we first derive $\Psi(\omega)$ assuming the signal spectrum is G_v only. Then with $S_\theta(\omega) = G_v$ and $D = T_e \lambda_v$,

$$|\Psi(\omega)|^2 = 1 + \frac{(N")^{-1} \sinh (D)}{\cosh (D) - \cos (\omega T)}, \tag{11}$$

and by analytic continuation in the S-plane we can form

$$\Psi(s)\ \Psi(-s) = \frac{\cosh (D) + (N")^{-1} \sinh (D) - \cosh (sT)}{\cosh (D) - \cosh (sT)}. \tag{12}$$

It is simple to factor (12) to get its poles and zeros (p-z). The p-z of (12) in the left half of the S-plane correspond to the p-z of $\Psi(\omega)\ \Psi^*(\omega)$ in the upper half of the ω-plane. Then $\Psi(s)$ is formed from the p-z of (12) in the left half S-plane. The poles of (12) follow by factoring cosh (sT) = cosh (D). These poles occur at

$$s = \frac{1}{T} [\pm D \pm j\ 2\pi n] \tag{13}$$

where n = 0, 1, 2, $\cdots$. The zeros follow from cosh (sT) = cosh (D) + $(N")^{-1}$ sinh (D). The zeros occur at

$$s = \frac{1}{T} [\pm \cosh^{-1} [\cosh (D) + (N")^{-1} \sinh (D)] \pm j\ 2\pi m] \tag{14}$$

where m = 0, 1, 2, $\cdots$. The p-z of $\Psi(s)\ \Psi(-s)$ are simple and countably infinite in the S-plane. The p-z of $\Psi(s)$ are those s values in (13) and (14) that have negative real parts as shown in Figure 4. The real part of the zeros is $-(1/T) \cosh^{-1} R$ where $R = \cosh D + (N")^{-1} \sinh (D)$.

Although there are an infinite number of poles and zeros for $\Psi(s)$ when we let $S_\theta(\omega) = G_v$, it is easy to show that a simple structure realizes the p-z of Figure 4. We find in Appendix III that $\Psi(s)$ is realized by the delay-line circuit (comb Filter) shown in Figure 5.

(2.6) The Optimum Loop Filter for $S_\theta(\omega) = G_h\ G_v$.

Substituting G_h and G_v from (7) and (8) we get

$$\Psi(\omega)\ \Psi^*(\omega) = 1 + S_\theta(\omega)/N'' =$$

$$1 + \frac{\lambda^2}{\omega^2+\lambda^2} \cdot (N^*)^{-1} \frac{\sinh(D)}{\cosh(D) - \cos(\omega T)}, \qquad (15)$$

where $\lambda = \lambda_h$, $D = T_e\ \lambda_v$, $\omega = 2\pi f$, $k = \overline{d^2} - \bar{d}^2$, and $N^* = N''\lambda_h/2k$. Using analytic continuation into the S-plane we get

$$\Psi(s)\ \Psi(-s) = \frac{(\lambda^2-s^2)\ [\cosh(D)-\cosh(sT)] + \lambda^2\ (N^*)^{-1}\ \sinh(D)}{(\lambda^2-s^2)\ [\cosh(D)-\cosh(sT)]} \qquad (16)$$

The poles and zeros of $\Psi(s)$ are the left-half S-plane roots of the denominator and numerator of (16), respectively. The constant parameters λ, D, T and N* are real and positive. Then we see that $\cosh(D) > 1$ and $\sinh(D) > D > 0$. If $\lambda \to +\infty$ and N* is held constant, the zeros of $\Psi(s)$ in (16) are the left-half S-plane roots of $\cosh(D) + (N^*)^{-1} \sinh(D) - \cosh(sT) = 0$. That is, the solution for $\Psi(s)$ in (16) converges to the solution found from (12) when $N^* = N''$.

In a practical situation we can assume that $\lambda_h >> T^{-1}$. That is, there are many oscillations of $S_\theta = G_h\ G_v$ between $\omega = 0$ and the half-power frequency $\omega = \lambda_h$ of the envelope G_h. This suggests that we find the zeros of $\Psi(s)$ in (16) using a computer search of the S-plane around the zeros shown in Figure 4.

The zeros of $\Psi(s)$ are solutions of the pair of simultaneous equations in x and y that result when $s = x + jy$ is substituted in the numerator of (16); and we equate real and imaginary parts to zero. The pair of simultaneous equations is (17).

$$(\lambda^2+y^2-x^2)\cosh(D) + (\lambda^2/N^*)\sinh(D) =$$

$$(\lambda^2+y^2-x^2)\cosh(xT)\cos(yT) + 2xy\sinh(xT)\sin(yT)$$

$$-2xy\cosh(D) = (\lambda^2+y^2-x^2)\sinh(xT)\sin(yT)$$

$$-2xy\cosh(xT)\cos(yT) \qquad (17)$$

Several properties of the solutions of (17) are apparent.

(i) If λ, D and T are held constant and $N^* \to +\infty$, the numerator approaches the denominator in (16), and $\Psi(s)$ approaches unity. On the real axis, $y = 0$ in (17), and the real roots are solutions of (18).

$$(\lambda^2-x^2)\cosh(D) + (\lambda^2/N^*)\sinh(D) = (\lambda^2-x^2)\cosh(xT) \qquad (18)$$

Because of the existance of two real negative roots of (18) as $N^* \to +\infty$, we expect to find more than one real negative root of (18) for finite N^*. The negative roots of (18) for $N^* \to +\infty$ are $x = -\lambda$ and $x = -D/T$.

(ii) Since cosh w and cos w are even functions of a real w while sinh w and sin w are odd functions of the argument, we find that if $s_o = x_o + jy_o$ is a solution of (17) then $-s_o$, s_o^* and $-s_o^*$ are also solutions where s_o^* is the conjugate of s_o.

(iii) Since $\Psi(\omega)\,\Psi^*(\omega) = 1 + S_\theta(\omega)/N''$ where $N'' > 0$ and $S_\theta(\omega) \geq 0$, there is no value of ω such that $\Psi(\omega) = 0$. That is, there are no imaginary roots of (17).

(2.7) Numerical Solution for $\Psi(\omega)$.

A special computer program was used to find solutions of (17) (Ref. 6). Two sets of signal parameters were considered corresponding to models for Broadcast Television (BCTV) and PICTUREPHONE Television (PPTV) (Ref. 3, Sec. 5,6).

For BCTV we used $\rho_v = \rho_h = 0.9$, $T_e/T = 0.00128$, and $T = 63 \times 10^{-6}$ sec. Since $\rho_v = \exp[-\lambda_v T_e] = \exp[-D] = 0.9$, we get $D = \ell n\,[1/0.9]$ and $\lambda = \lambda_h = T_e^{-1} D$. For PPTV we used $\rho_v = \rho_h = 0.9$, $T_e/T = 0.0041$, and $T = 63 \times 10^{-6}$ sec. Then for these cases the constants in (17) were

$$\text{BCTV:} \begin{cases} D = \ell n\,[1/0.9] \\ T = 63 \times 10^{-6} \text{ sec.} \\ \lambda = 12.4 \times 10^{6}\, D \\ N^* = \dfrac{\alpha \sinh(D)}{\cosh(D) - 1}, \ \alpha \text{ a parameter to be assigned.} \end{cases}$$

$$\text{PPTV:} \begin{cases} D = \ell n\,[1/0.9] \\ T = 63 \times 10^{-6} \text{ sec.} \\ \lambda = 3.84 \times 10^{6}\, D \\ N^* = \dfrac{\alpha \sinh(D)}{\cosh(D) - 1} \end{cases}$$

The values of α were selected to give a broad range of signal-to-noise ratios. We note that $S_\theta(0) = \sinh(D)/[\cosh(D) - 1]$. Then

$$S_\theta(0)/N^* = 1/\alpha. \tag{19}$$

We used the values $\alpha \times 10^4 = 7.5$, 10, 25, 50, and 75 corresponding to signal-to-noise density ratios at $\omega = 0$ between 1.33×10^2 and 1.33×10^3 in (19).

The graphs of the first 100 zeros of (17) in the upper-left quadrant of the S-plane are shown in Figures 6 and 7 corresponding to BCTV and PPTV, respectively. In each figure the locus of zeros varies with the parameter α. For each α there is one real zero at the x intercept of the locus of zeros. A second real zero of (18) also exists for each combination of values of α and λ. For all values of α and λ considered here, this second real zero was very close to $-\lambda$. The effect of this zero is canceled by the pole of $\Psi(s)$ that exists at $-\lambda$.

We see that as the imaginary part of the zero position increases the real part approaches -D/T which is the locus of the poles of $\Psi(s)$. We find that the zeros and poles of $\Psi(s)$ effectively cancel beyond the first hundred or so. This cancellation is reasonable since the signal spectrum $S_\theta(\omega)$ tends to zero as ω approaches $\pm\infty$ while the noise density N* is fixed. When the noise becomes large compared to the signal, the optimum filter $H_o(s)$ must approach zero. A zero transfer function $H_o(s)$ is obtained when $\Psi(s) = 1$. But $\Psi(s) = 1$ when all zeros and poles cancel and the gain constant of $\Psi(s)$ is unity.

(2.8) Synthesis of a Transfer Function to Approximate $\Psi(s)$.

The synthesis of the transfer function $\psi(s)$ when $S_\theta(\omega) = G_h\, G_v$ appears to be very difficult. However, the transmission poles of $\Psi(s)$ are the same as the poles in equation (13). Hence the poles of our $\psi(s)$ are realized by the transfer function from (3) to (4) in Figure 5. There is a pole of $\Psi(s)$ at $s = -\lambda$, but as we pointed out before this pole is canceled very well by a zero of $\psi(s)$ near $-\lambda$, for the values of the parameters we consider.

Since the simple feedforward transfer function from points (2) to (3) in Figure 5 can generate zeros on a line parallel to the j-axis at intervals $j2\pi n/T$, $n = 0, \pm 1, \pm 2, \cdots$, it seems there should be some technique for altering the circuit in Figure 5 to get the transmission zeros shown in Figures 6 and 7. Several alterations of the feedforward transfer function (2) to (3) in Figure 5 were investigated. We changed the transfer function (2) to (3) to $F_i(s)$, i = 1, 2, 3, shown in Figure 8 where

$$G_1(s) = K\,\omega_o/(s+\omega_o),$$

$$G_2(s) = K\,s/(s+\omega_h),$$

and
$$G_3(s) = K(s+a)/(s+\omega_h), \tag{20}$$

with $0 \leq a \leq \omega_h$, and $0 \leq k \leq 1$.

The effect of $G_1(s)$ is to cause the zeros of the transfer function $F_1(s)$ in Figure 8 to move away from the j-axis as we increase $|\omega|$. The effect of $G_2(s)$ is to cause the zeros of the transfer function $F_2(s)$ to approach $-\infty$ as $|\omega|$ approaches zero. Neither of these effects approximate the zero locations in Figures 6 and 7 very well. However, if $G_3(s)$ is used we can adjust K, a and ω_h for each combination of α and λ such that the zeros of $F_3(s)$ in Figure 8 are close to those in Figures 6 and 7.

Since $G_3(s)$ approaches K for large $|s|$ and since $K = e^{-D}$, where $D = \ell n\,[1/0.9]$ for the loci in Figures 6 and 7, we know that $F_3(s)$ can give us an accurate approximation for the transfer zeros only if $K = 0.9$. With this value for K we selected a and ω_h to get the best approximation of the zeros of $\Psi(s)$ for each combination of α and λ.

When (20) is used in Figure 8 we get

$$F_3(s) = \frac{s + \omega_h - K\,(s+a)\,e^{-ST}}{s + \omega_h} \tag{21}$$

The finite zeros of $F_3(s)$ follow from (21) by substituting $s = x + jy$ and solving for solution pairs (x, y) in the system of equations

$$\begin{aligned} x + \omega_h - K\,(x+a)\,e^{-xT}\cos(yT) - Kye^{-xT}\sin(yT) &= 0 \\ y - Kye^{-xT}\cos(yT) + K\,(x+a)\,e^{-xT}\sin(yT) &= 0 \end{aligned} \tag{22}$$

The program used to find the solutions of (17) was also used to solve (22).

In Figure 6 we show the zeros of $F_3(s)$ with corresponding ω_h and a that best approximate the zeros of $\Psi(s)$ in the BCTV case for α values between 0.75×10^{-3} and 7.5×10^{-3}. For each α we search for ω_h and a that minimize the maximum magnitude of the difference of the real parts of the zeros of $\Psi(s)$ and $F_3(s)$ over the first 100 zeros of $\Psi(s)$. The optimization based on only the real parts of the zeros of $\Psi(s)$ and $F_3(s)$ is meaningful, since the differences in the imaginary parts of the zeros of $\Psi(s)$ and $F_3(s)$ are approximately zero in the cases we consider (see Figure 6).

The transfer function (21) has two zeros on the negative real axis and a real pole at $s = -\omega_h$. As we see from 22 with $y = 0$, the two real zeros are the solutions of the real equation

$$e^{-xT} = (x+\omega_h)/(x+a)\ K = f(x). \tag{23}$$

The two solutions of 23 are shown in Figure 9. For the values of ω_h, T, K and a we use in $F_3(s)$ to approximate the zeros of $\Psi(s)$ in the BCTV and PPTV cases, the most negative real zero $-a'$ is almost equal to $-a$.

We may write (21) in the form

$$F_3(s) = \left(\frac{s+a'}{s+\omega_h}\right) \cdot F_3^{\dagger}(s) \tag{24}$$

where $F_3^{\dagger}(s)$ has a countable number of finite transmission zeros along a locus in the S-plane for each combination of ω_h, T, K and a as shown in Figure 6. Then a transfer function that closely approximates the countable number of isolated zeros of $\Psi(s)$ when $S_\theta(\omega) = G_h\ G_v$ is just

$$F_3^{\dagger}(s) = \left(\frac{s+\omega_h}{s+a'}\right)\ F_3(s) \tag{25}$$

and it is obtained by preceeding the filter shown in Figure 8 by the new filter $(s+\omega_n)/(s+a')$.

(2.9) Suboptimum PLL Demodulators

Using (25) to approximate the transmission zeros of $\Psi(s)$ we get a suboptimum transfer function $\Psi_a(s)$ shown in Figure 10. We introduce a gain C in $\Psi_a(s)$ since we must specify the gain constant of a transfer function in addition to its pole and zero positions. The value that C must have follows from a simple argument. Since the optimum filter $H_o(j\omega)$, for the mms error estimate of $\theta(t)$ given $\theta(t)$ + noise, must approach zero as $\omega \to \pm\infty$ whenever $\lim S_\theta(\omega)/N'' = 0$ as $\omega \to \pm\infty$, we have $\lim \Psi(j\omega) = 1$ as $\omega \to \pm\infty$. Our approximation $\Psi_a(j\omega)$ approaches $\Psi(j\omega)$ as $\omega \to \pm\infty$. Then

$$\lim_{\omega \to \pm\infty} \Psi_a(s) = 1 = C, \tag{26}$$

and C = 1 in Figure 10.

If we substitute the suboptimum filter $\Psi_a(s)$ for $\Psi(s)$ in equation 1, we get a suboptimum filter H(s) in place of $H_o(s)$. The suboptimum H(s) is shown in Figure 11. This follows from equation 1 and Figure 10.

It was pointed out that for the parameters of the BCTV and PPTV cases a' and a are nearly equal. If we set a' = a for the system in Figure 11, we get the simple result shown in Figure 12. The loop filter in Figure 12 is just the cascade of a simple feedback delay and an RC lowpass filter.

(2.10) Minimum Error Optimization of a and ω_h for the Suboptimum Demodulator.

Deriving a simple circuit with poles and zeros approximately equal to those of the optimum $\Psi(s)$ discussed in section 2.6 is an intuitively pleasing attack on the suboptimum filter problem, indeed it was consideration of the zero loci of $\Psi(s)$ that led to the circuits in Figures 11 and 12. However, the criterion for optimization we are using is mms error. For the assumed suboptimum

filter structure in Figure 12 the values of a, K, T and ω_h that produce a mms error estimate of $\theta(t)$ are not necessarily those that minimize the distances between the zero positions and the pole positions of $\Psi(s)$ and $\Psi_a(s)$.

For any filter H(s) used to estimate $\theta(t)$ given $\theta(t) + n'(t)/A$, the mean square error is given by

$$\sigma^2 = \frac{1}{2\pi} \int_{-\infty}^{+\infty} |1-H(j\omega)|^2 \, S_\theta(\omega) \, d\omega + \frac{1}{2\pi} \int_{-\infty}^{+\infty} |H(j\omega)|^2 \, N''(\omega) \, d\omega, \qquad (27)$$

where $S_\theta(\omega)$ and $N''(\omega)$ are the power spectral densities of $\theta(t)$ and $n'(t)/A$, respectively (Ref. 7, Equation 7-87). Then we can substitute $H(j\omega)$ from Figure 12 and minimize σ^2 with respect to the circuit parameters a, ω_h, K and T. This search was performed over a and ω_h with K = 0.9 and T = 63 x 10^{-6} for both BCTV and PPTV cases.

The system in Figure 12 is realizable, and we derive for this structure the optimum a and ω_h for mms error given K and T. The mms error in estimating $\theta(t)$ using the optimum realizable linear filter is given by (4). We compare the optimum realizable linear filter with the circuit in Figure 12 as follows. For different values of subcarrier signal power, σ_θ^2, we plot σ_θ^2/σ^2 and $\sigma_\theta^2/\sigma_o^2$ vs. 1/N". For each value of parameter σ_θ^2 and independent variable 1/N" we compute σ_o^2 from (4) and σ^2 from (27), where (27) is minimized with respect to a and ω_h. We define $\sigma_\theta^2/\sigma_o^2$ and σ_θ^2/σ^2 to be the optimum and suboptimum demodulator output signal-to-noise power ratios, respectively.

The subcarrier signal power is

$$\sigma_\theta^2 = \frac{1}{2\pi} \int_{-\infty}^{+\infty} S_\theta(\omega)\, d\omega$$

$$= k \int_{-\infty}^{+\infty} \frac{2\lambda}{\omega^2+\lambda^2} \cdot \frac{\sinh (T_e \lambda)}{\cosh (T_e \lambda) - \cos \omega T} \cdot \frac{d\omega}{2\pi}$$

$$= k \cdot 1 \qquad (28)$$

That is, $\sigma_\theta^2 = k$ (Ref. 3, Appendix B). We note that $N'' = N_o/2A^2$ and hence our independent variable is $1/N'' = 2A^2/N_o$. This is the ratio of signal power A^2 to noise spectral density $N_o/2$ at the demodulator input.

The optimum demodulator output SNR is

$$\sigma_\theta^2/\sigma_o^2 = \frac{k}{\frac{N''}{\pi} \int_0^{+\infty} \ell n\, [1 + S_\theta(\omega)/N'']\, d\omega}$$

$$= \frac{\lambda/2}{\frac{N^*}{\pi} \int_0^{+\infty} \ell n\, [1 + S_{\theta^*}(\omega)/N^*]\, d\omega} \qquad (29)$$

where $$N^* = \frac{\lambda N''}{2k}$$

and $$S_{\theta^*}(\omega) = \frac{\lambda^2}{\omega^2+\lambda^2} \cdot \frac{\sinh (D)}{\cosh (D) - \cos \omega T}$$

The suboptimum demodulator output SNR is

$$\sigma_\theta^2/\sigma^2 = \frac{k}{\frac{1}{\pi}\int_0^{+\infty} |1-H(\omega)|^2 S_\theta(\omega)\, d\omega + \frac{1}{\pi}\int_0^{+\infty} N''\, |H(\omega)|^2\, d\omega}$$

$$= \frac{\lambda/2}{\frac{1}{\pi}\int_0^{+\infty} |1-H(\omega)|^2 S_{\theta *}(\omega)\, d\omega + \frac{1}{\pi}\int_0^{\infty} N^*\, |H(\omega)|^2\, d\omega} \qquad (30)$$

Figures 13, 14, 15, and 16 are families of $\sigma_\theta^2/\sigma_0^2$ and σ_θ^2/σ^2 for the BCTV and PPTV cases. In each figure the family parameter is the subcarrier signal power k. Figures 17 and 18 give the values of ω_h that optimized the circuit in Figure 12 for each value of k and 1/N". For the BCTV case the value of a was approximately constant at 3×10^6. Similarly for PPTV the value of a was approximately $(0.9) \times 10^6$.

(2.11) Stability of the Suboptimum Demodulator

For the linear circuit in Figure 12 it is relatively easy to find the conditions for which the closed loop transfer function H(s) is stable. It should be obvious that we need stability in our demodulator if it is to perform its task properly.

The open loop transfer function for Figure 12 is

$$G(s) = \frac{\omega_h - a}{s+a} \cdot \frac{1}{1 - K \exp[-sT]}. \qquad (31)$$

This is not a rational function of s, and any stability test that applies to feedback systems that have rational open loop transfer functions must be extended to include (31). The stability test we use for our demodulator is a general Nyquist criterion. This criterion and the proof of stability for Figure 12 are presented in Appendix IV. The condition for stability of the demodulator in Figure 12 is that $\omega_h - a > 0$ and $0 \leq k < 1$.

(3.0) RESULTS AND CONCLUSIONS

We have developed a tractable suboptimum phase locked loop demodulator that estimates a TV type signal phase modulated on the received carrier. For the two sets of signal parameters used, BCTV and PPTV, it was found that the suboptimum PLL demodulator phase estimates had mean square errors not much larger than the mms errors theoretically possible considering all realizable linear internal loop filters for the demodulator. These results can be seen in the graphs of $\sigma_\theta^2/\sigma_o^2$ and σ_θ^2/σ^2 for the BCTV and PPTV cases.

The suboptimum PLL demodulator was derived by first searching for the transmission poles and zeros of the optimum demodulators internal loop filter. This search was performed using a special computer program to find the real and imaginary components of the loop filter poles and zeros. For the phase modulation spectrum model used, the optimum internal loop filter had a countably infinite number of poles and zeros. A filter possessing the optimum poles and zeros has not been found; it seems to be a formidable synthesis problem.

The suboptimum PLL demodulator was obtained by trial and error starting from a simple internal loop filter that contained time delayed feedback. By augmenting this basic internal loop filter with an RC network, we obtained a simple internal loop filter with transmission poles identical to those of the optimum loop filter and with transmission zeros close to the optimum zero positions.

The suboptimum internal loop filter was developed using the circuit theory approach of approximating the optimum pole-zero constellation by a tractable suboptimum constellation. However, since the performance criterion used was minimum mean square error estimation by the PLL demodulator, the circuit parameters for the suboptimum PLL demodulator were adjusted to get minimum mean square phase estimation error. This parameter optimization was made possible by the mean square error expression in (27) that is valid for suboptimum as well as optimum demodulators.

The graphs of the optimum and suboptimum output SNR ratios $\sigma_\theta^2/\sigma_o^2$ and σ_θ^2/σ^2 are plotted with respect to the demodulator input signal power-to-noise power density ratio $2A^2/N_o = 1/N"$. The family parameter in each case is the average power $\sigma_\theta^2 = k$ of the modulation $\theta(t)$. For any given family, we

find that the member curves are the same except that they are shifted along the 1/N" axis as k is changed. This behavior is apparent from the normalized equations (29) and (30). If we initially calculate $\sigma_\theta^2/\sigma_o^2$ or σ_θ^2/σ^2 for normalized values of N*, the resulting curve is translated along the 1/N" axis by changing the values of k in $1/N" = \lambda/2kN^*$ where the λ are fixed for the BCTV and PPTV cases. The same characteristic applies to the families of ω_h plotted with respect to 1/N" with k as a parameter. The value of a is essentially constant at 3×10^6 for BCTV and 0.9×10^6 for PPTV.

The stability of the suboptimum PLL demodulator while in its linear range of operation was investigated using a generalized Nyquist criterion applicable to the nonrational loop filter transfer function. The condition for stability obtained was $0 \leq K < 1$ under the assumption $\omega_h - a > 0$ made at the outset of our derivation. The condition $0 \leq K < 1$ is also the requirement for open loop stability of the suboptimum demodulator. The suboptimum demodulator we have derived is valid only when the PLL is in lock such that we can make the assumption that $\theta(t) - \hat{\theta}(t) \approx 0$. The stability analysis we performed is based on this linear assumption. When the PLL demodulator is not in lock we have not shown that it will lock up. That is, nothing has been said about the stability of the demodulator when it is not locked onto the modulated signal. A solution to this nonlinear stochastic acquisition problem is not known at this time.

W. D. Wynn

2034-WDW-pjr

Attachment
Figures 1-19
Appendices I-IV

REFERENCES

1. "Optimum Angle Modulation," C. J. Boardman and H. L. Van Trees, IEEE Trans. Comm. Theory, December 1965, pp. 452-469.

2. "Low-Resolution TV: Subjective Effects of Noise Added to a Signal," R. C. Brainard, The Bell System Technical Journal, January 1967, pp. 233-260.

3. "A Model for the Random Video Process," L. E. Franks, The Bell System Technical Journal, April 1966, pp. 609-630.

4. Principles of Coherent Communication, A. J. Viterbi, McGraw-Hill Book Co., New York, 1966.

5. Detection, Estimation, and Modulation Theory, Part I, H. L. Van Trees, John Wiley and Sons, Inc., New York, 1968.

6. "Parametric Analysis Program," P. F. Long, TM-70-1032-1, Bellcomm, Inc., Washington, D. C., January 1970.

7. Communication Theory: Transmission of Waveforms and Digital Information, D. J. Sakrison, John Wiley and Sons, Inc., New York, 1968.

8. "A General Formulation of the Nyquist Criterion," C. A. Desoer, IEEE Trans. on Circuit Theory, June 1965, pp. 230-234.

9. Mathematical Analysis, T. M. Apostol, Addison-Wesley Publishing Company, Inc., Reading Mass., 1957.

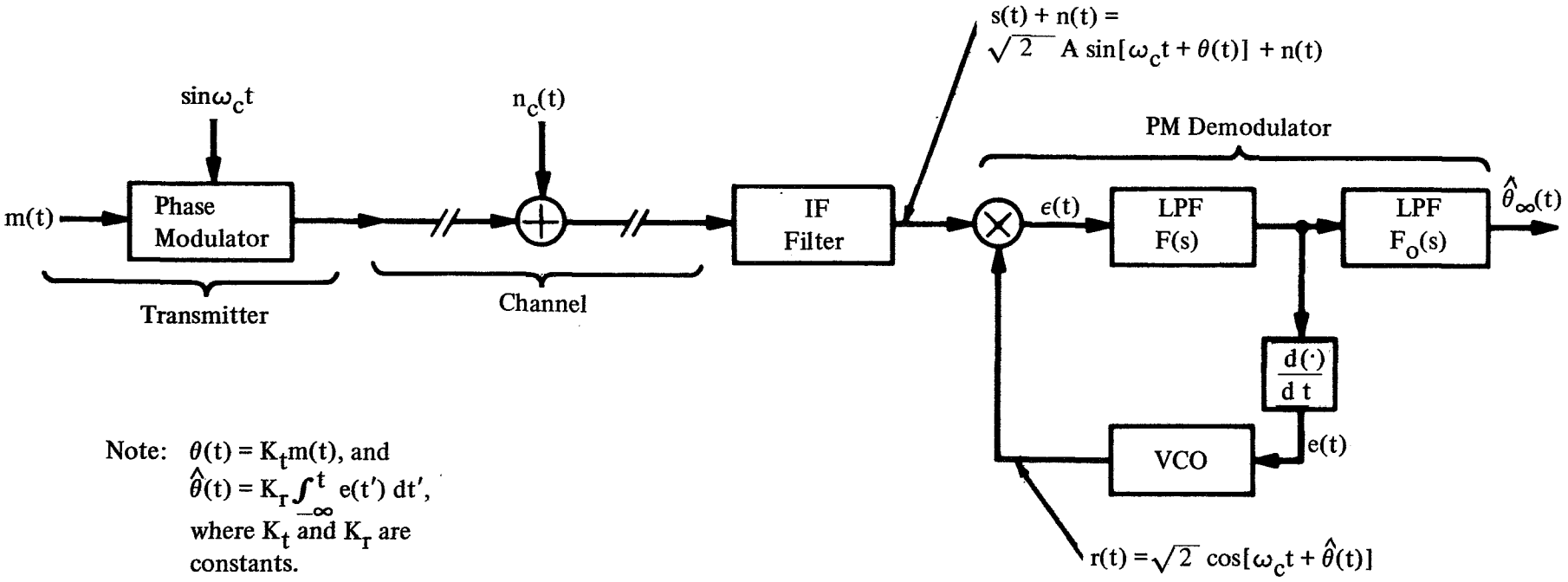

Note: $\theta(t) = K_t m(t)$, and
$\hat{\theta}(t) = K_r \int_{-\infty}^{t} e(t')\, dt'$,
where K_t and K_r are constants.

FIGURE 1 - A BASIC PHASE MODULATION COMMUNICATION SYSTEM

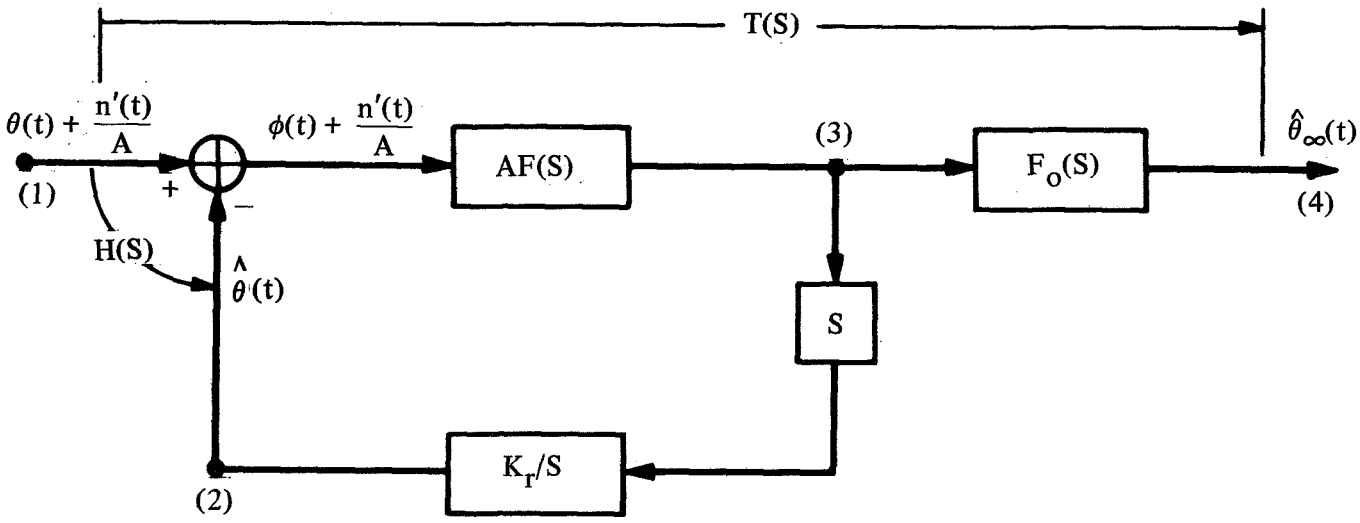

FIGURE 2 - THE ABOVE THRESHOLD – LOWPASS EQUIVALENT FOR THE PLL–PM DEMODULATOR

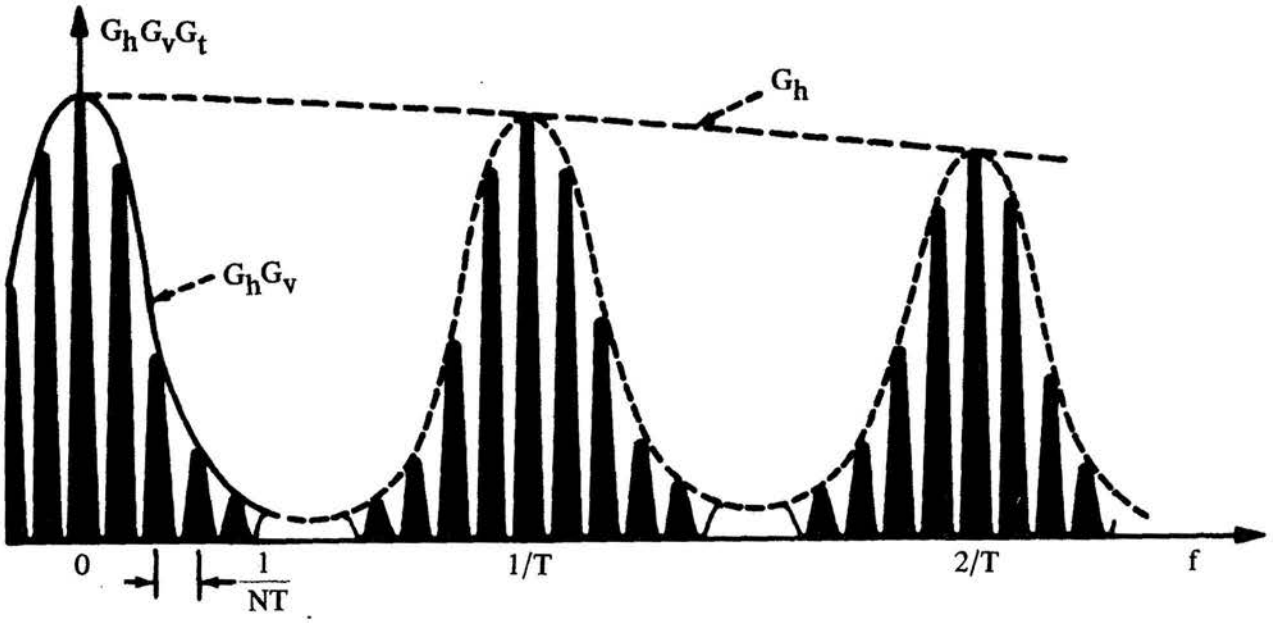

FIGURE 3 - POWER SPECTRAL DENSITY OF VIDEO SIGNAL WITH FRAME-TO-FRAME CORRELATION, QUALITATIVE PLOT OF $G_h(f)G_v(f)G_t(f)$

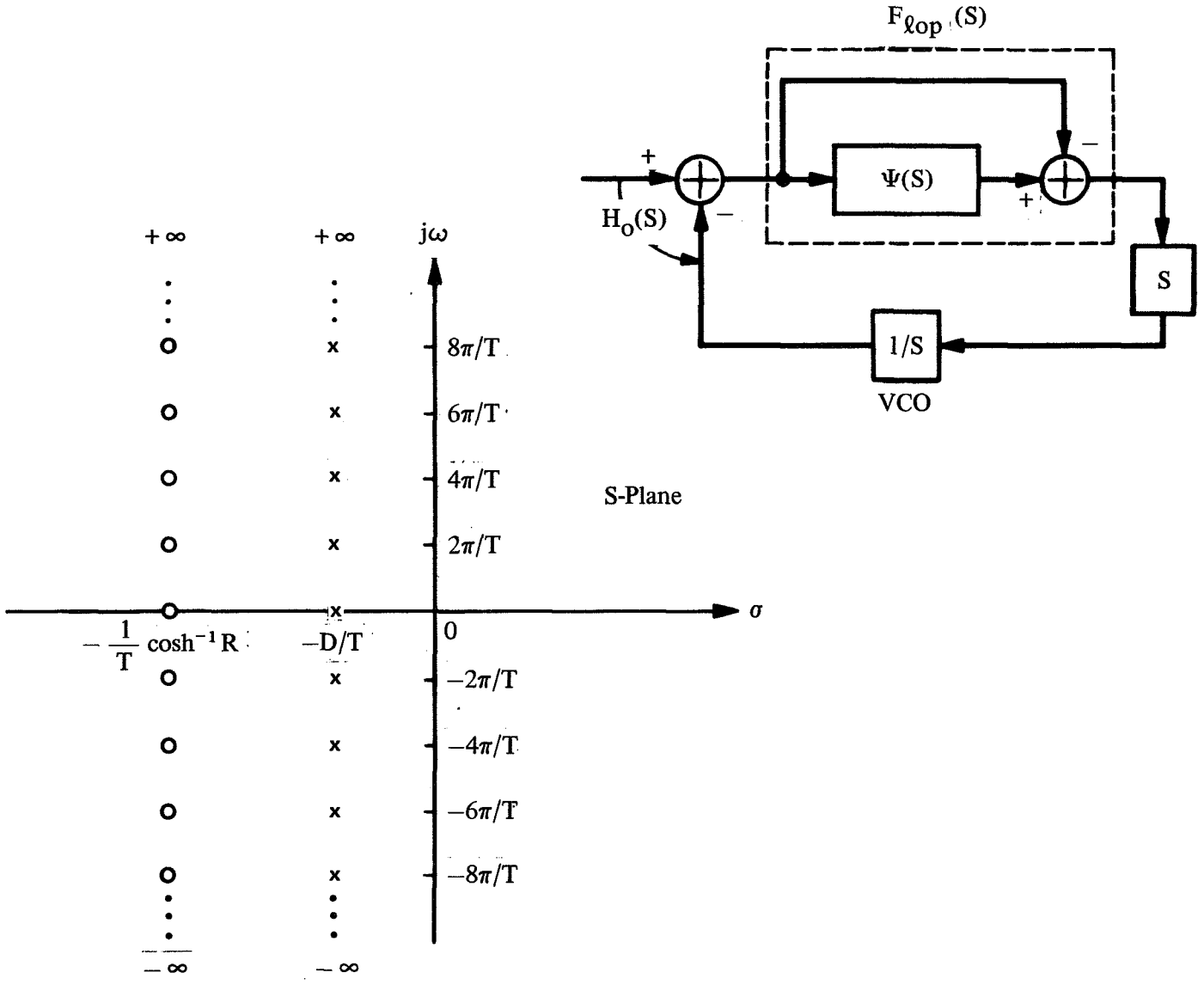

FIGURE 4 - POLE-ZERO POSITIONS OF $\Psi(S)$ FOR THE OPTIMUM $F_{\ell op}(S)$

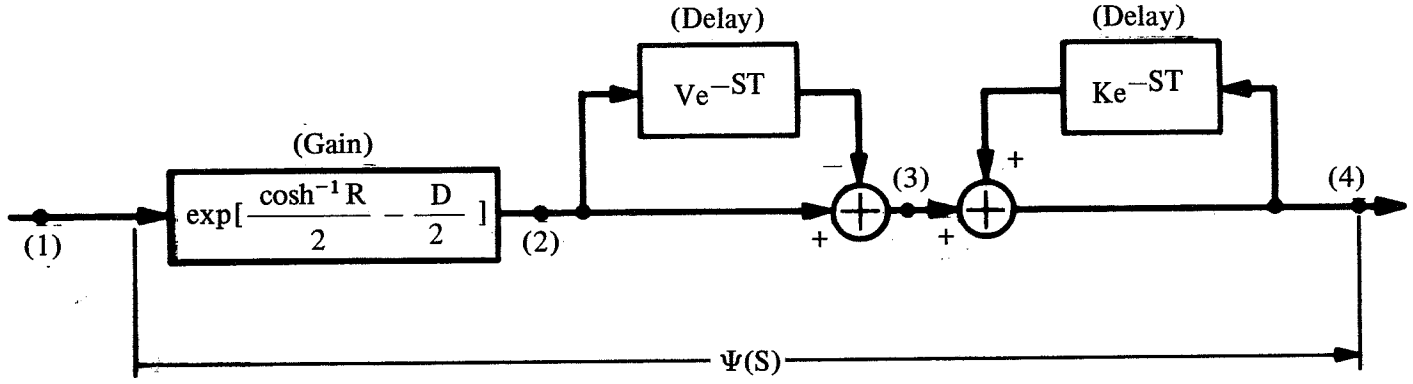

FIGURE 5 - A FEEDBACK REALIZATION OF $\Psi(S)$ WHEN $S_\theta(\omega) = G_v$

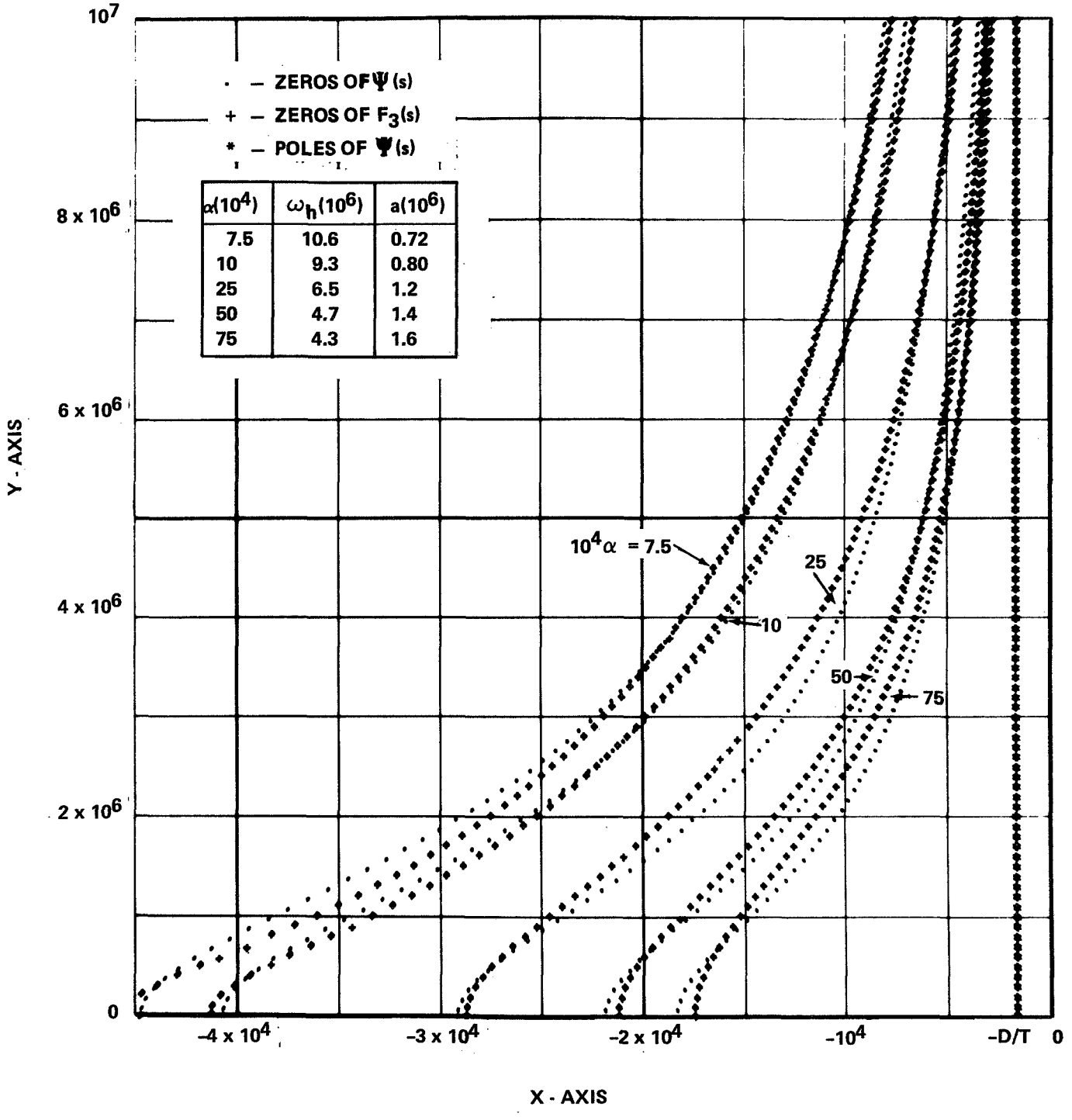

FIGURE 6 - POLES AND ZEROS OF $\Psi(s)$ AND $F_3^{\dagger}(s)$ IN UPPER-LEFT QUADRANT OF THE S-PLANE FOR BCTV PARAMETERS AND $\alpha = 0.75 \times 10^{-3}$, 10^{-3}, 2.5×10^{-3}, 5×10^{-3}, AND 7.5×10^{-3}.

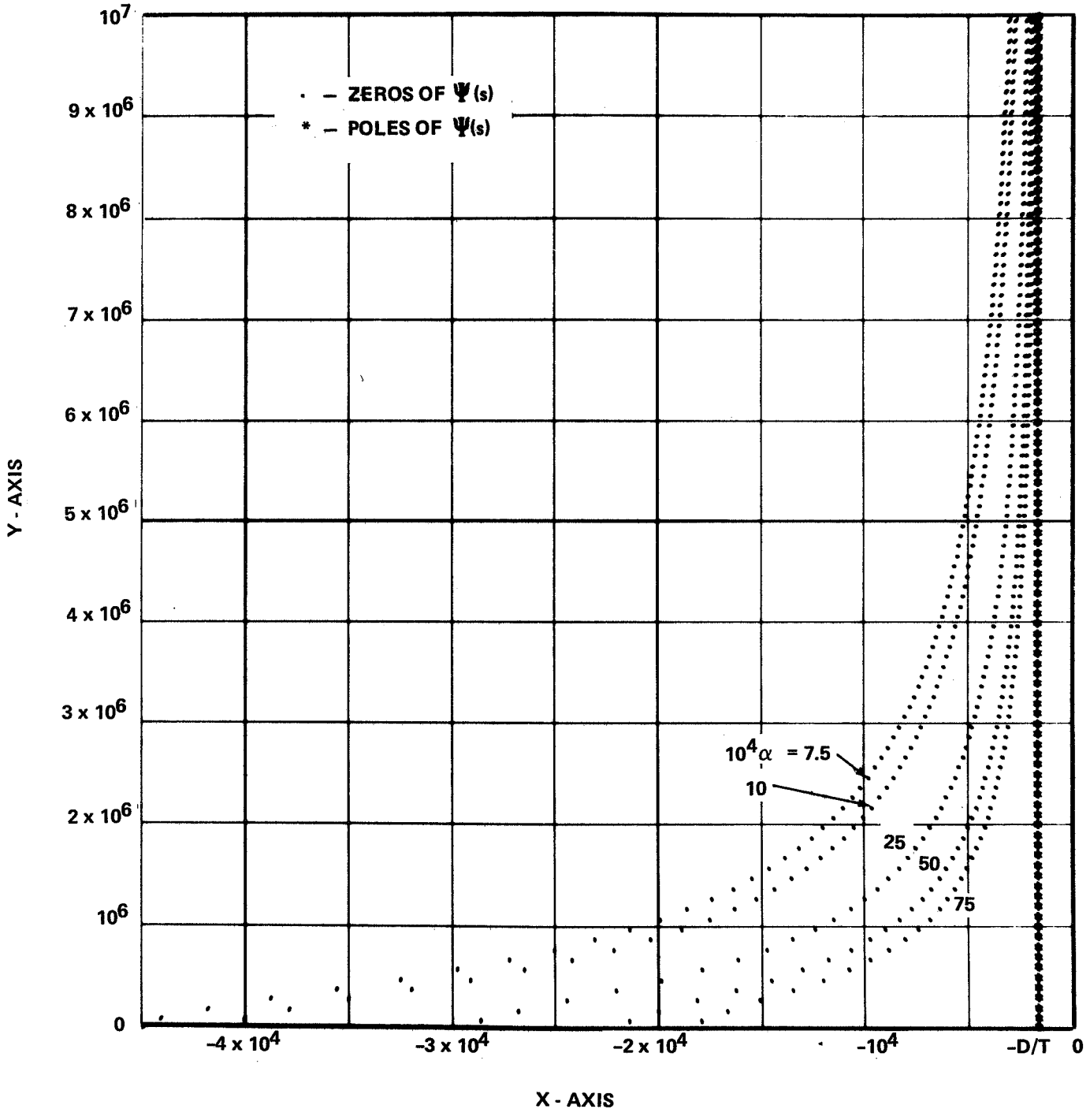

FIGURE 7 - ZEROS OF $\Psi(s)$ IN THE UPPER-LEFT QUADRANT OF THE S-PLANE FOR PPTV PARAMETERS AND $\alpha = 0.75 \times 10^{-3}, 10^{-3}, 2.5 \times 10^{-3}, 5 \times 10^{-3}$, AND 7.5×10^{-3}.

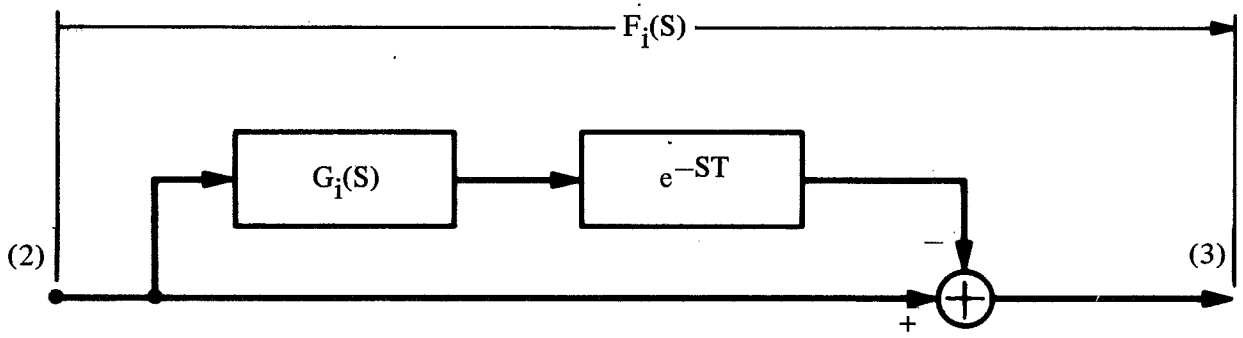

FIGURE 8 - A FEEDFORWARD TRANSFER FUNCTION FOR APPROXIMATE SYNTHESIS OF THE ZEROS OF $\Psi(S)$ WHEN $S_\theta(\omega) = \overline{G_h} G_v$ (i = 1,2,3)

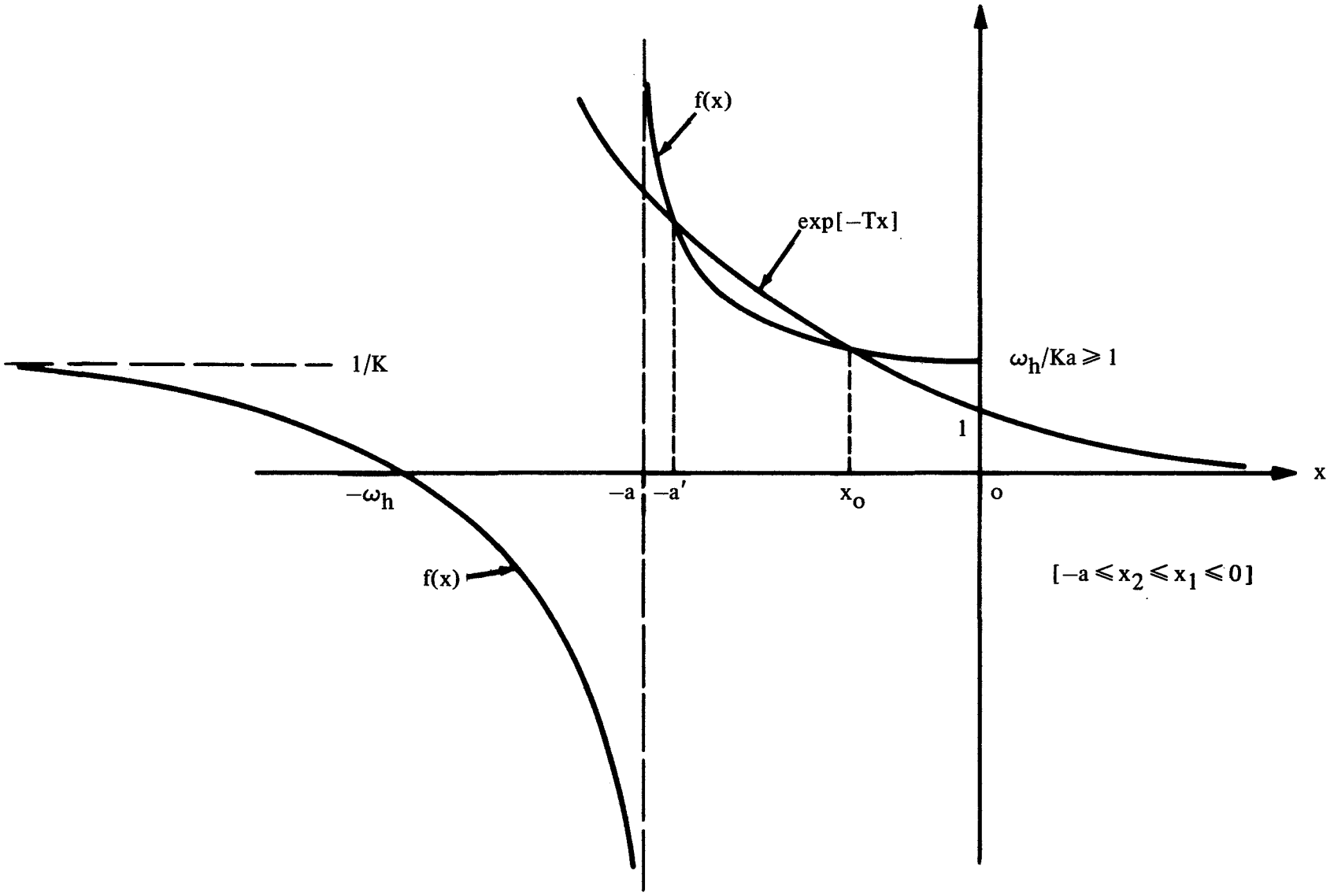

FIGURE 9 - GRAPHICAL SOLUTION FOR THE TWO REAL ROOTS OF $F_3(S)$

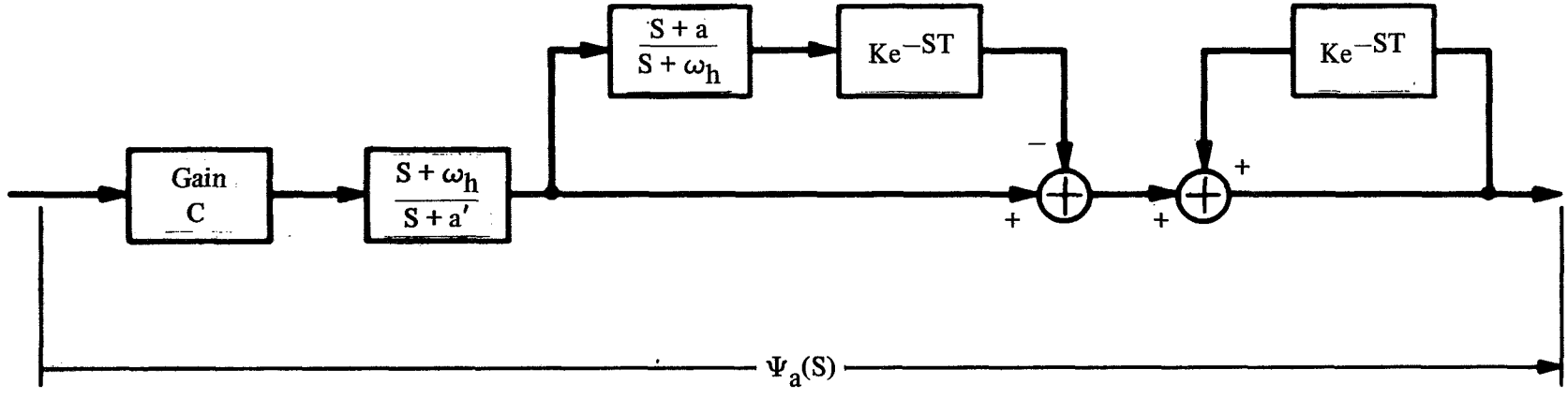

FIGURE 10 - A SUBOPTIMUM FILTER THAT APPROXIMATES $\Psi(S)$

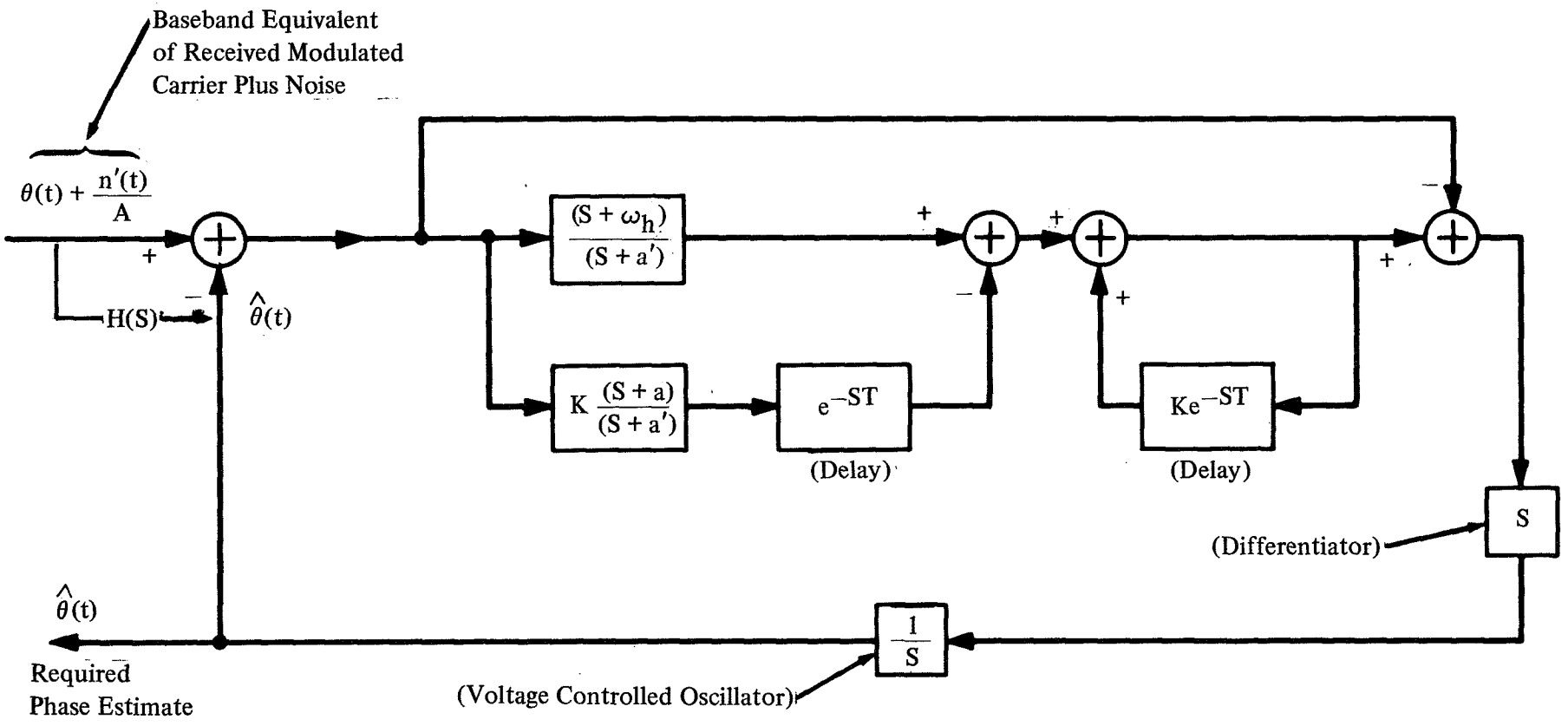

FIGURE 11 - THE ABOVE-THRESHOLD BASEBAND EQUIVALENT PHASE LOCKED LOOP TV DEMODULATOR

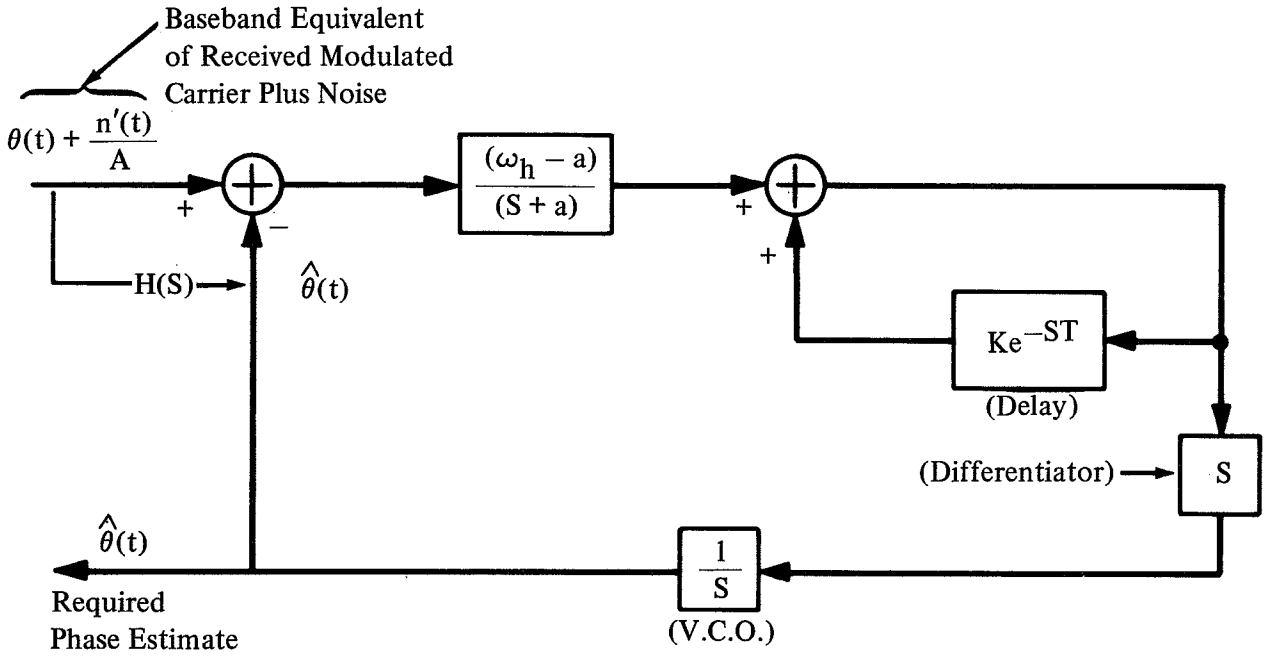

FIGURE 12 - THE REDUCED FORM FOR THE DEMODULATOR IN FIGURE 11 WHEN a = a′

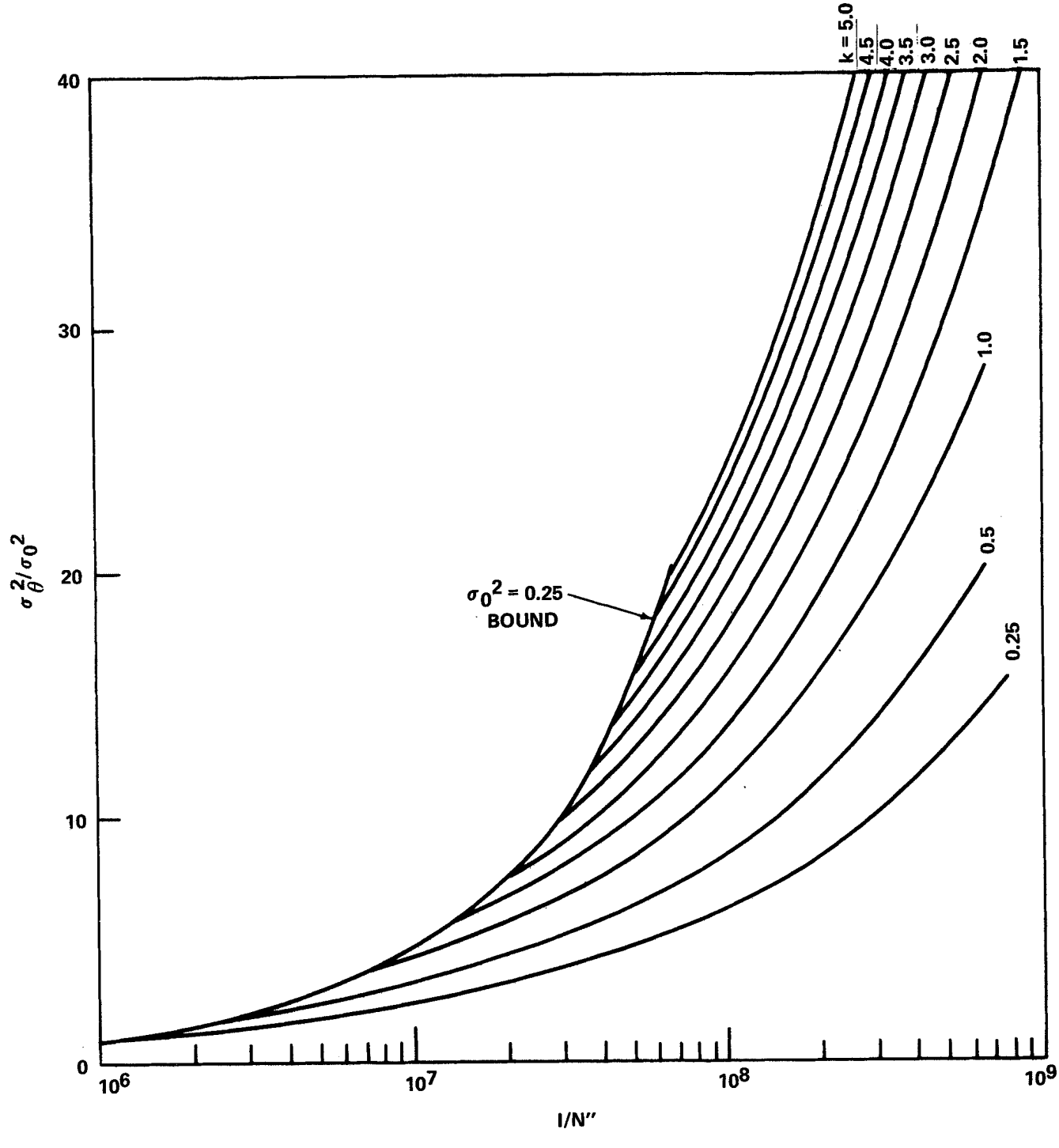

FIGURE 13 - OPTIMUM SIGNAL-TO-NOISE RATIO CURVES FOR THE BCTV CASE. ($\sigma_0^2 \leq 0.25$)

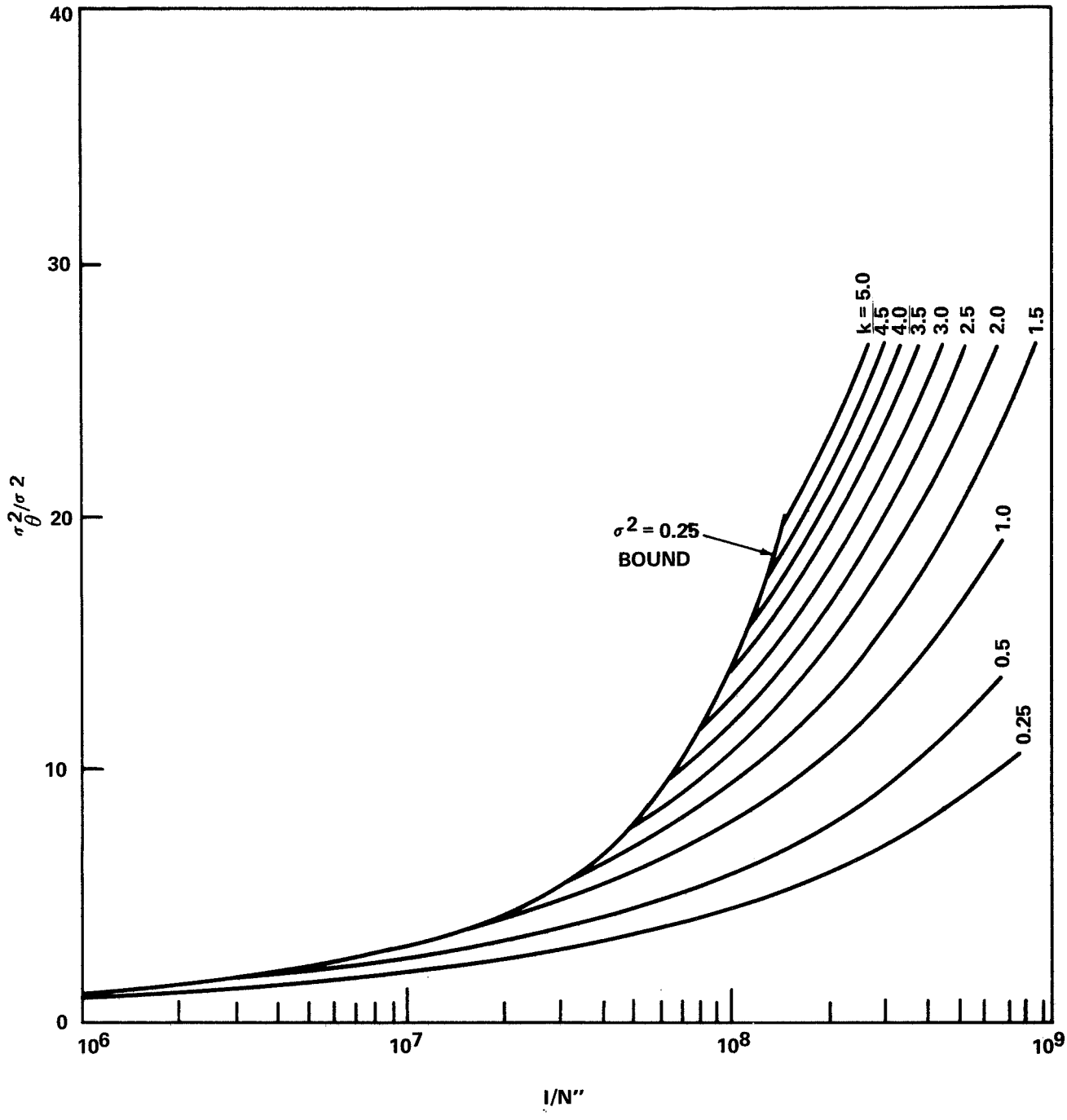

FIGURE 14 - SUBOPTIMUM SIGNAL-TO-NOISE RATIO CURVES FOR THE BCTV CASE. ($\sigma^2 \leq 0.25$)

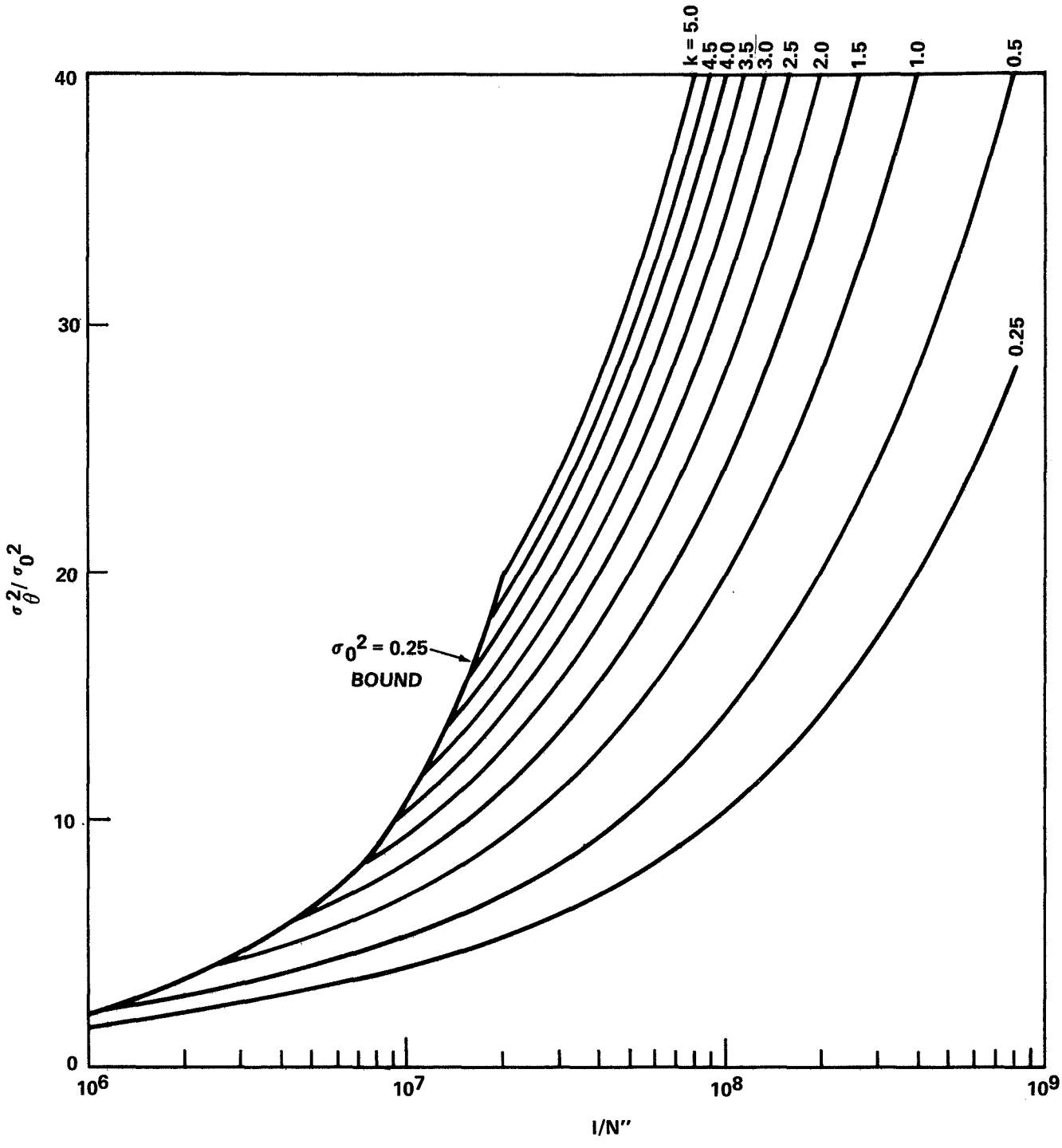

FIGURE 15 - OPTIMUM SIGNAL-TO-NOISE RATIO CURVES FOR PPTV CASE. ($\sigma_0^2 \leq 0.25$)

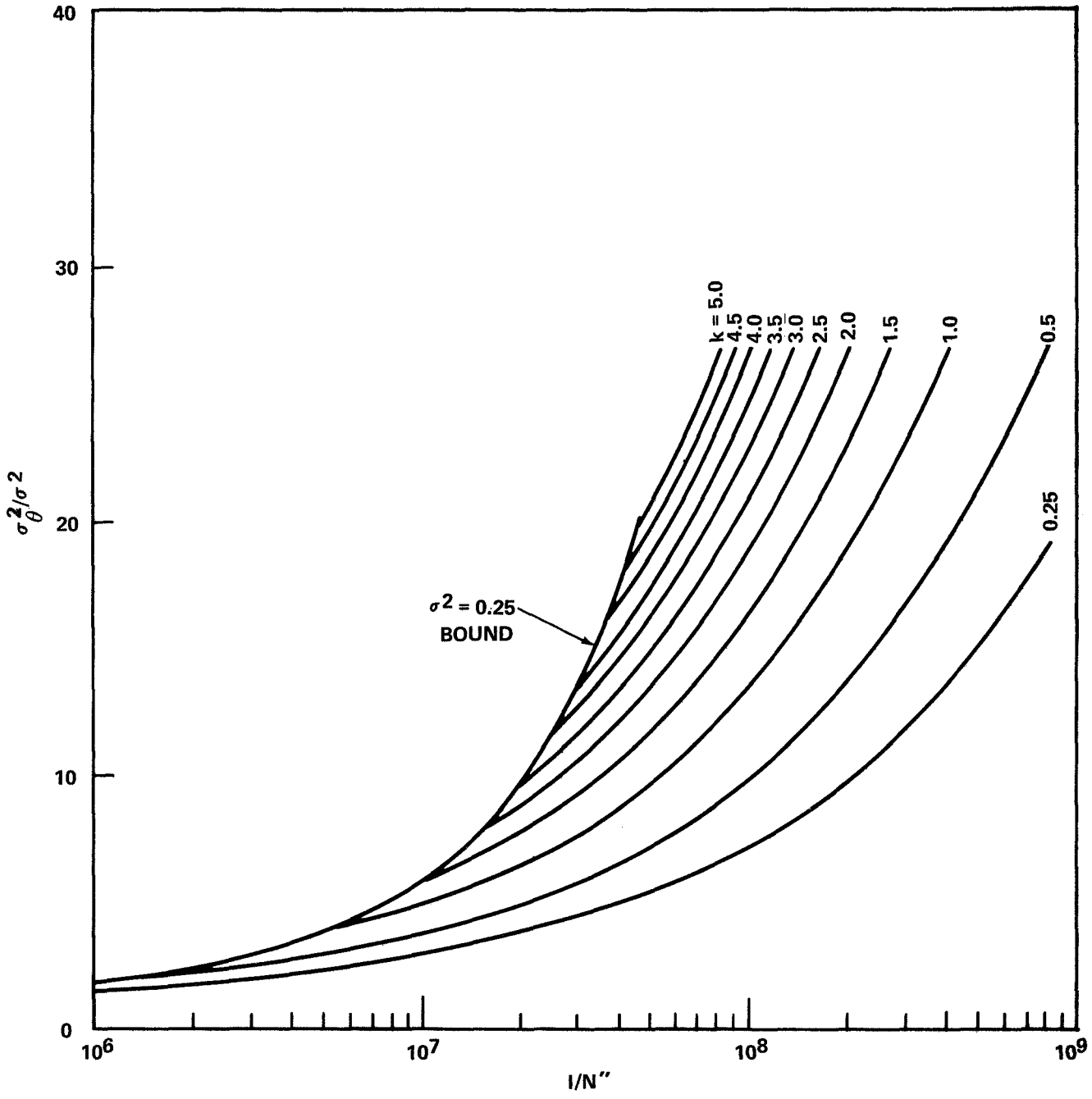

FIGURE 16 - SUBOPTIMUM SIGNAL-TO-NOISE RATIO CURVES FOR PPTV CASE. ($\sigma^2 \leq 0.25$)

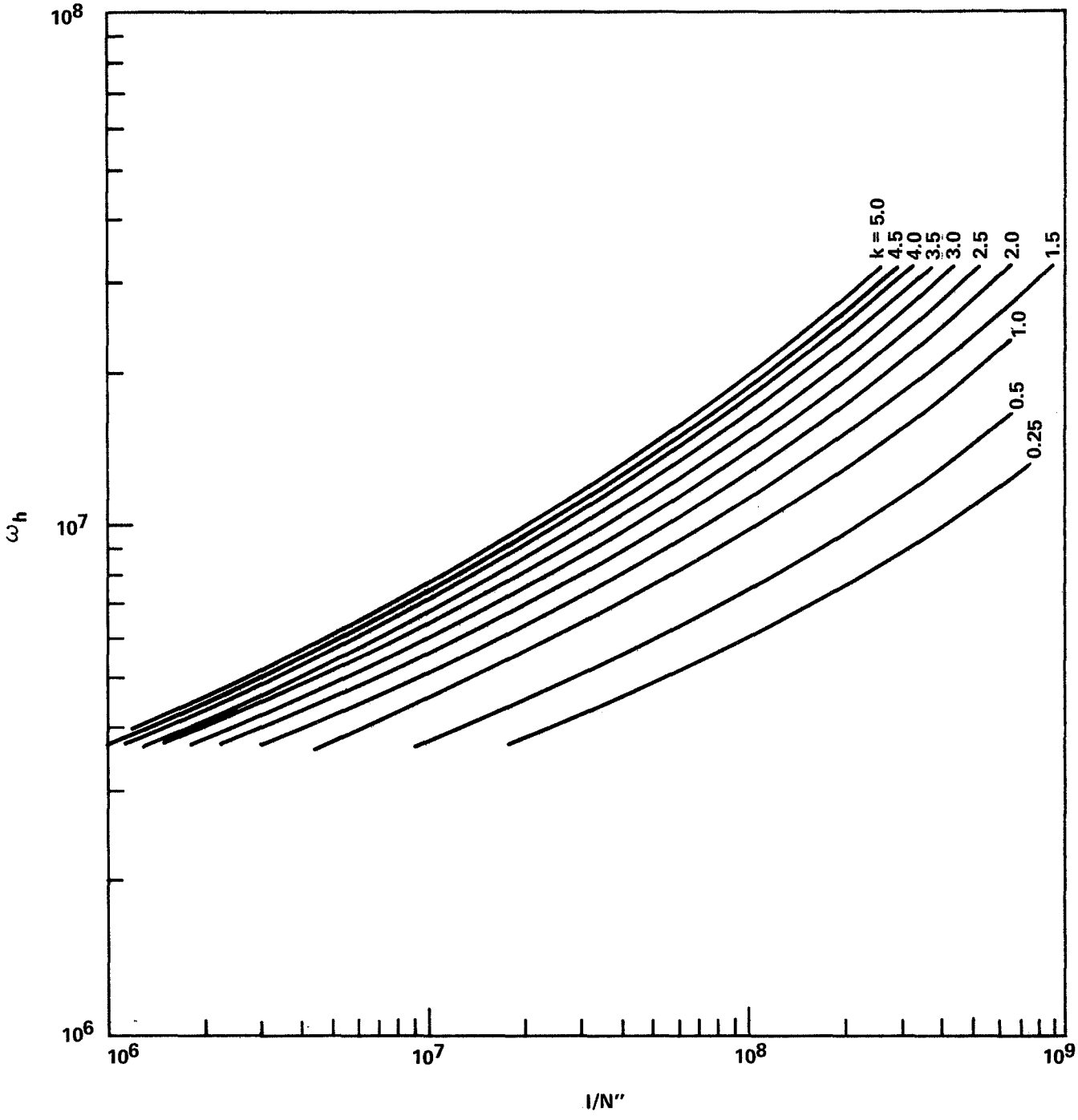

FIGURE 17 - VARIATIONS IN ω_h vs. $2A^2/N_0$ FOR BCTV CASE.

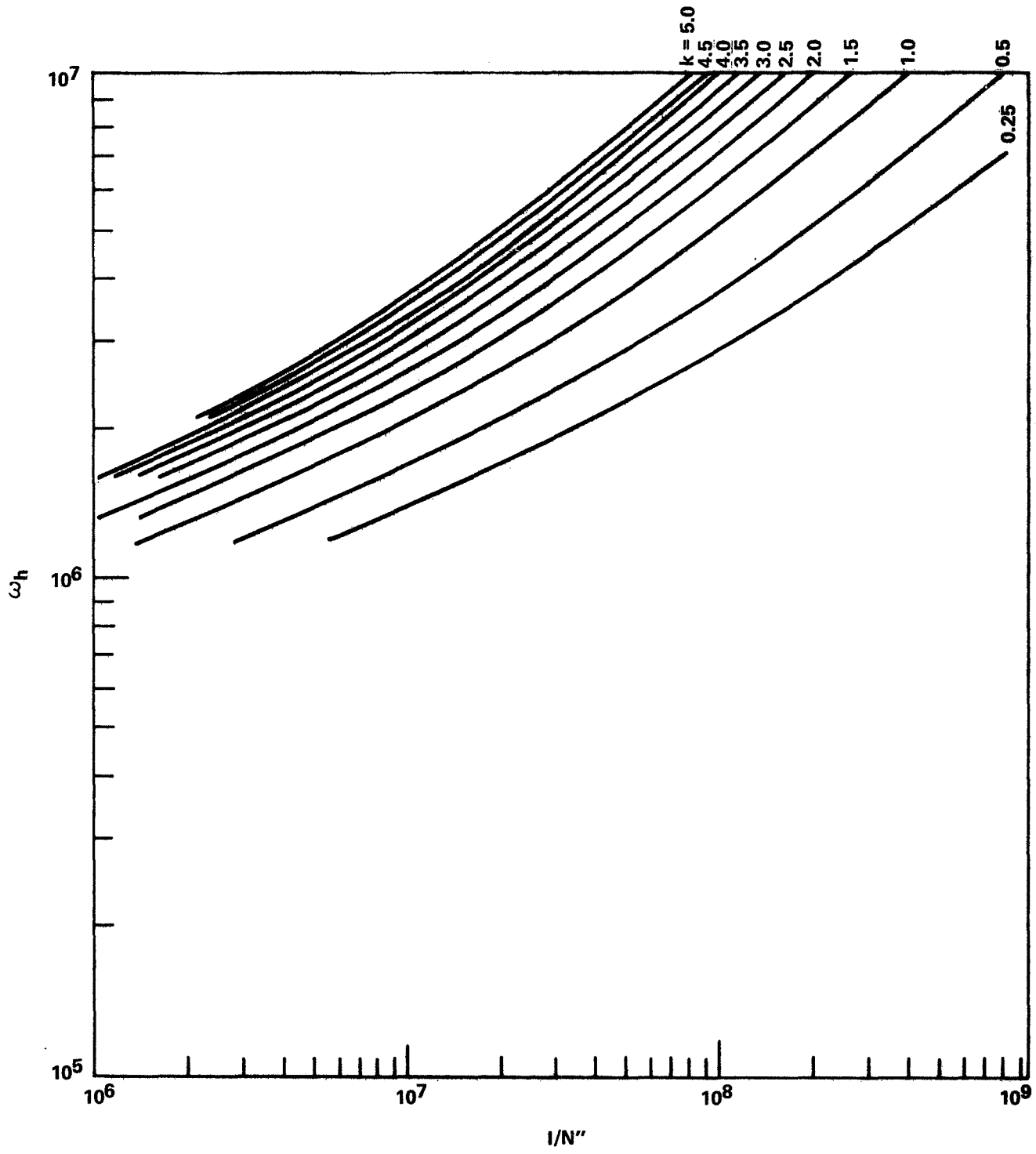

FIGURE 18 - VARIATIONS IN ω_h vs. $2A^2/N_0$ FOR PPTV CASE.

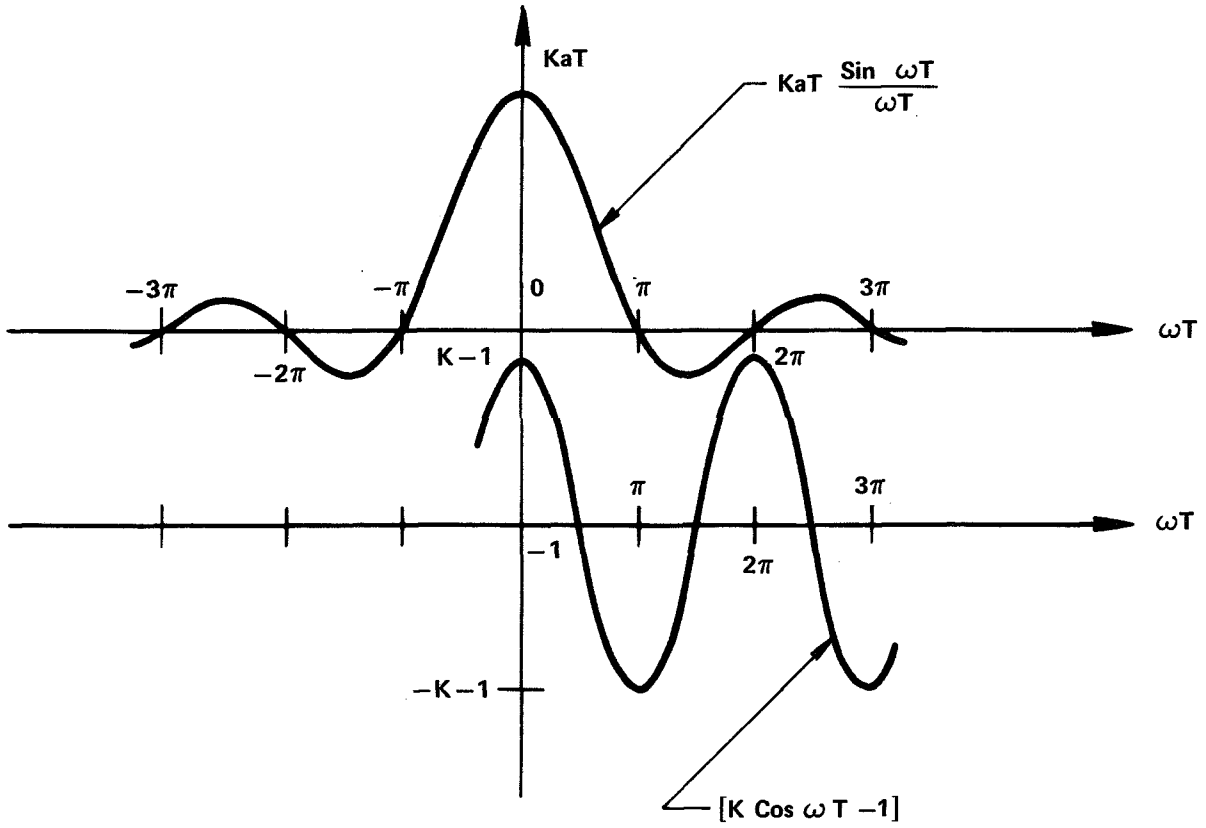

FIGURE 19 – GRAPHICAL SOLUTION OF ZEROS OF Im [G (jω)]

APPENDIX I

THE OPTIMUM POST LOOP FILTER WITH LONG DELAY

When no time delay is permitted in estimating $\theta(t)$, the optimum post loop filter is $F_o(s) = K_r$. Then the estimates at points (2) and (4) in Figure 2 are identical. With sufficiently long time delay allowed in $F_o(s)$ we can approach $\hat{\theta}_\infty(t)$ and the error in the estimate is approximately the irreducible mms error. The post loop filter with delay is a realizable filter that can be derived from $F_{\ell op}(j\omega)$ and $T_o(j\omega)$, where $T_o(j\omega)$ is the unrealizable Wiener filter that yields the absolute mms error estimate $\hat{\theta}_\infty(t)$. The unrealizable Wiener filter is given by

$$T_o(j\omega) = \frac{S_\theta(\omega)}{S_\theta(\omega) + N''} \overset{\mathcal{F}}{\leftrightarrow} t_o(t) \tag{A-1}$$

where $\mathcal{F}$ is the Fourier transform operation. For any signals $\theta(t)$ we will consider here, the impulse response $t_o(t)$ of the unrealizable filter (4) tends to zero as $t \to \pm\infty$. Then if $\delta > 0$ is sufficiently large, the impulse response of the filter

$$T_o(j\omega)\, e^{j\omega\delta} \overset{\mathcal{F}}{\leftrightarrow} t_o(t-\delta) \tag{A-2}$$

is close to zero for all $t < 0$. We can use the realizable filter

$$G_o(j\omega) \overset{\mathcal{F}}{\leftrightarrow} g_o(t) = \begin{cases} t_o(t-\delta), & t \geq 0 \\ 0, & t < 0 \end{cases} \tag{A-3}$$

in place of $T_o(j\omega)$, and the realizable estimate we get with $g_o(t)$ will approach $\hat{\theta}_\infty(t)$ as $\delta \to +\infty$.

With $T_o(j\omega)$ replaced by $G_o(j\omega)$ the optimum realizable output filter with delay δ is

$$F_{oop}(j\omega) = G_o(j\omega) \cdot \frac{K_r}{H_o(j\omega)} \qquad \text{(A-4)}$$

where $H_o(j\omega)$ and $G_o(j\omega)$ are given by (1) and (A-3).

APPENDIX II

DEFINITION OF TERMS IN THE TV SIGNAL MODEL

The parameters contained in random signal parts of $S(\omega)$ are defined as follows.

(i) $\overline{d^2} - \bar{d}^2$ = Variance of luminance of the picture.

(ii) T_e = Time interval equivalent to the distance between adjacent lines at beam scanner velocity.

(iii) λ_h, λ_v = Poisson rate parameters describing luminance process in the horizontal and vertical directions, respectively.

(iv) T = line scan interval in seconds, i.e., the time from start of a line to start of next line.

(v) N = Number of lines per frame.

(vi) λ_t = Poisson rate parameter describing luminance process frame-to-frame.

Given the values of N, T, and T_e, the values of λ_h, λ_v and λ_t follow from the expressions

$$\rho_h = \exp(-\lambda_h T_e), \quad \rho_v = \exp(-\lambda_v T_e) \qquad \text{(A-5)}$$

and

$$\rho_t = \exp(-\lambda_t NT)$$

where the ρ's are determined emperically. Usually N and T are known and T_e is found from the ratio T_e/T. This is the procedure used in L. E. Franks' Paper.

APPENDIX III

The transfer zeros and poles of the $\Psi(s)$ in Figure 5 are generated separately by the transfer functions from points (2) to (3) and (3) to (4), respectively, when we properly specify V and K. To show that this is true we consider the transfer functions

$$G(s) = \frac{1}{1 - K \exp [-st_\ell]}, \quad 0 \leq K \leq 1 \qquad \text{(A-6)}$$

and

$$V(s) = 1 - V \exp [-st_\ell], \quad 0 \leq V \leq 1 \qquad \text{(A-7)}$$

The function G(s) has only finite poles and V(s) has only finite zeros. The poles of G(s) are

$$s = \frac{-1}{t_\ell} \ell n \ (1/K) \pm j \frac{2\pi n}{t_\ell}, \quad n = 0, 1, \cdots,$$

and the zeros of V(s) are

$$s = \frac{-1}{t_\ell} \ell n \ (1/V) \pm j \frac{2\pi m}{t_\ell}, \quad m = 0, 1, \cdots.$$

The pole positions of G(s) are the same as the pole positions of $\Psi(s)$ in (13) when $t_\ell = T$ and $\ell n \ (1/K) = D$ or $K = \exp [-D]$. The zeros of V(s) are the same as the zeros of $\Psi(s)$ in (14) when $t_\ell = T$ and $\ell n \ (1/V) = \cosh^{-1} R$ or $V = \exp [-\cosh^{-1} R]$ where $R = \cosh (D) + (N")^{-1} \sinh (D)$.

Consider next the product

$$(1-Ke^{-ST})\ (1-Ke^{+ST}) = 2K\left[\frac{1+K^2}{2K} - \cosh\ (ST)\right]$$

$$= 2e^{-D}\ [\cosh\ (D) - \cosh\ (ST)]$$

$$= 2e^{-D} \times \text{Denominator of } \Psi(s)\ \Psi(-s)$$

since $K = e^{-D}$. Also

$$(1-Ve^{-ST})\ (1-Ve^{+ST}) = 2V\left[\frac{1+V^2}{2V} - \cosh\ (ST)\right]$$

$$= 2\ \exp\ [-\cosh^{-1}\ (R)]\ [R-\cosh\ (ST)]$$

$$= 2\ \exp\ [-\cosh^{-1}\ (R)] \times \text{Numerator of } \Psi(s)\ \Psi(-s)$$

$$\text{Then } \Psi(s) = \frac{\exp\left[\frac{1}{2}\cosh^{-1}\ (R)\right]}{\exp\left[\frac{1}{2}\ D\right]} \cdot \frac{(1-Ve^{-ST})}{(1-Ke^{-ST})} \qquad \text{(A-8)}$$

APPENDIX IV

A GENERAL NYQUIST CRITERION AND THE STABILITY CONDITIONS FOR FIGURE 12.

With respect to the demodulator in Figure 12 we can summarize the general Nyquist criterion (Ref. 8) as follows.

Theorem: If the impulse response $g(t)$ of $G(s)$ is given by

$$g(t) = u_{-1}(t)\ g_1(t) \tag{A-9}$$

where $u_{-1}(t)$ is the unit step at $t = 0$ and if

(i) $g_1(t)$ is bounded on $[0, \infty)$,

(ii) $g_1(t) \in L^1(0, \infty)$, i.e. $g_1(t)$ is absolutely integrable on $[0, \infty)$,

(iii) $g_1(t) \to 0$ as $t \to +\infty$,

and (iv) The Nyquist diagram of $G(s)$ does not encircle or go through the critical point $(-1, 0)$ in the $G(s)$ plane; then

(a) The impulse response of the closed loop feedback system in Figure 12 is bounded, tends to zero as $t \to +\infty$ and is an element of $L^1(0, \infty)$, and

(b) For any bounded input, the response of the closed loop system is bounded.

From the convolution theorem (Ref. 9, Sec. 15-18) and result (a) of the above theorem it also follows that when (a) holds and any absolutely integrable function on $(-\infty, \infty)$ is applied to the closed loop feedback system containing $G(s)$, the response is a unique, well-defined function.

If the results (a) and (b) are to hold for Figure 12, we must show that our g(t) in (31) satisfies (A-9) and that $g_1(t)$ satisfies conditions (i) through (iv). For K < 1 the impulse response of G(s) is

$$g(t) = \mathcal{L}^{-1}\left[\frac{\omega_h - a}{s+a} \cdot \frac{1}{1 - K \exp[-sT]}\right]$$

$$= \mathcal{L}^{-1}\left[\frac{\omega_h - a}{s+a} \cdot \sum_{n=0}^{\infty} K^n \exp[-snT]\right]$$

$$= \sum_{n=0}^{\infty} K^n \int_{-\infty}^{\infty} \beta(\tau)\, u_o(t-nT-\tau)\, d\tau$$

$$= \sum_{n=0}^{\infty} K^n\, \beta(t-nT) \qquad \text{(A-10)}$$

where $u_o(t-nT)$ is the unit impulse at $t = nT$, and

$$\beta(t) = \mathcal{L}^{-1}\left[\frac{\omega_h - a}{s+a}\right] = (\omega_h - a)\, e^{-at}\, u_{-1}(t) \geq 0. \qquad \text{(A-11)}$$

We see that $g(t) = 0$ for $t < 0$, hence g(t) has the form in (A-9). Consider now

$$\int_0^{\infty} |g_1(t)|\, dt = \int_0^{\infty} \left| \sum_{n=0}^{\infty} K^n\, \beta(t-nT) \right| dt =$$

$$(\omega_h - a) \int_0^\infty \sum_{n=0}^\infty K^n \, e^{-a(t-nT)} \, u_{-1}(t-nT) \, dt =$$

$$(\omega_h - a) \sum_{n=0}^\infty K^n \int_0^\infty e^{-a(t-nT)} \, u_{-1}(t-nT) \, dt =$$

$$(\omega_h - a) \sum_{n=0}^\infty K^n \cdot \frac{1}{a} = \frac{\omega_h - a}{a} \cdot \frac{1}{1-K} \qquad \text{(A-12)}$$

Then if $0 \leq K < 1$, $g_1(t) \in L^1(0, \infty)$, and condition (ii) is satisfied. If $0 \leq K < 1$, $g_1(t)$ is also bounded on $[0, \infty)$ and $\lim_{t \to \infty} g_1(t) = 0$. Then we only need to satisfy condition (iv) to show stability for the demodulator in Figure 12 when $0 \leq K < 1$. Consider then the Nyquist diagram of G(s). We substitute $s = j\omega$ to get

$$G(j\omega) = \frac{\omega_h - a}{(j\omega + a)} \cdot \frac{1}{1 - K \cos \omega T + j K \sin \omega T}$$

$$= \frac{(\omega_h - a) A - j(\omega_h - a) B}{A^2 + B^2} \qquad \text{(A-13)}$$

where $A = a - Ka \cos \omega T - K\omega \sin \omega T$

and $B = \omega - K\omega \cos \omega T + Ka \sin \omega T$

The Nyquist diagram of G(s) is obtained by plotting the real and imaginary parts of (A-13) in the complex plane. Since we require $0 \leq K < 1$, there are no values of ω where (A-13) becomes unbounded. For $\omega \to \pm\infty$, $G(j\omega) \to 0$, and for $\omega \to 0$, $G(j\omega) \to (\omega_h - a)/a(1-K) > 0$. If $G(j\omega)$ does encircle or pass through the critical point (-1, 0) we must have real axis crossings for the Nyquist diagram that are less than or equal to -1. We now consider the real axis crossings of $G(j\omega)$.

For $G(j\omega)$ to have a real axis crossing we must have its imaginary part equal to zero. Then let

$$\frac{-j(\omega_h - a)\ B}{A^2 + B^2} = 0 \qquad \text{(A-14)}$$

This implies $B = 0$ since A and B are bounded for finite ω and $\omega_h - a \neq 0$. Then

$$K \cos \omega T - 1 = \frac{KaT \sin \omega T}{\omega T} \qquad \text{(A-15)}$$

Figure 19 shows typical plots of the left and right sides of (A-15). The ωT values where the two plots intersect are substituted into (A-13) to get the real axis cross points.

Since $0 \leq K < 1$, any intersections of the two graphs of $K \cos \omega T - 1$ and $KaT \sin \omega T/\omega T$ can only occur for $|\omega T|$ in the intervals $[(2m-1)\pi, 2m\pi]$, $m = 1, 2, \cdots$. Consider then the real part of $G(j\omega)$ given by $A(\omega_h - a)/(A^2 + B^2)$. We noted earlier that $0 < A^2 + B^2 < +\infty$ for $0 \leq K < 1$. Also, $(\omega_h - a) > 0$. Then the sign of the real part of $G(j\omega)$ is the same as the sign of A. But

$$\begin{aligned} A &= a(1 - K \cos \omega T) - K\omega \sin \omega T \\ &= a(1 - K \cos \omega T) - \frac{K}{T}(\omega T)^2 \frac{\sin \omega T}{\omega T} \end{aligned} \qquad \text{(A-16)}$$

The imaginary part of $G(j\omega)$ can be zero for ωT other than 0 and $\pm\infty$ only when $\sin \omega T/\omega T \leq 0$. But for such values of ωT, A will be positive, since $a > 0$ and $0 \leq K < 1$. We can conclude that the critical point $(-1, 0)$ cannot be enclosed or intersected by the Nyquist curve of $G(s)$. Then the demodulator in Figure 12 is stable for $\omega_h - a > 0$ and $0 \leq K < 1$.